Article:

Powley, HR, Krom, MD and Van Cappellen, P (2018) Phosphorus and nitrogen trajectories in the Mediterranean Sea (1950–2030): Diagnosing basin-wide anthropogenic nutrient enrichment. Progress in Oceanography, 162. pp. 257-270. ISSN 0079-6611

https://doi.org/10.1016/j.pocean.2018.03.003

Phosphorus and nitrogen trajectories in the Mediterranean Sea (1950-2030):

Diagnosing basin-wide anthropogenic nutrient enrichment

Helen R. Powley[1*], Michael D. Krom[1,2,3], Philippe Van Cappellen[1]

[1]Ecohydrology Research Group, Water Institute and Department of Earth and Environmental Sciences, University of Waterloo, Waterloo, Ontario N2L 3G1, Canada

[2]School of Earth and Environment, University of Leeds, Leeds LS2 9JT, United Kingdom

[3]Department of Marine Biology, Charney School of Marine Sciences, University of Haifa, Mt Carmel, Haifa, Israel

*Corresponding author: hrpowley@uwaterloo.ca

Submitted to Progress in Oceanography

Keywords:

Mediterranean Sea, phosphorus, nitrogen, nutrient enrichment, thermohaline circulation, primary production

Highlights

- Marine derived sources dominate nutrient P and N inputs to the Mediterranean Sea
- Land derived P and N inputs increase by up to a factor of 3 between 1950 and 2030
- Variable circulation hinders detection of anthropogenic nutrient enrichment
- Changes in DON concentrations yield the most prominent anthropogenic signatures

Abstract:

Human activities have significantly modified the inputs of land-derived phosphorus (P) and nitrogen (N) to the Mediterranean Sea (MS). Here, we reconstruct the external inputs of reactive P and N to the Western Mediterranean Sea (WMS) and Eastern Mediterranean Sea (EMS) over the period 1950 to 2030. We estimate that during this period the land derived P and N loads increased by factors of 3 and 2 to the WMS and EMS, respectively, with reactive P inputs peaking in the 1980s but reactive N inputs increasing continuously from 1950 to 2030. The temporal variations in reactive P and N inputs are imposed in a coupled P and N mass balance model of the MS to simulate the accompanying changes in water column nutrient distributions and primary production with time. The key question we address is whether these changes are large enough to be distinguishable from variations caused by confounding factors, specifically the relatively large inter-annual variability in thermohaline circulation (THC) of the MS. Our analysis indicates that for the intermediate and deep water masses of the MS the magnitudes of changes in reactive P concentrations due to changes in anthropogenic inputs are relatively small and likely difficult to diagnose because of the noise created by the natural circulation variability. Anthropogenic N enrichment should be more readily detectable in time series concentration data for dissolved organic N (DON) after the 1970s, and for nitrate (NO_3) after the 1990s. The DON concentrations in the EMS are predicted to exhibit the largest anthropogenic enrichment signature. Temporal variations in annual primary production over the 1950-2030 period are dominated by variations in deep-water formation rates, followed by changes in riverine P inputs for the WMS and atmospheric P deposition for the EMS. Overall, our analysis indicates that the detection of basin-wide anthropogenic nutrient concentration trends in the MS is rendered difficult due to: 1) the Atlantic Ocean contributing the largest reactive P and N inputs to the MS, hence diluting the anthropogenic nutrient signatures, 2) the anti-estuarine circulation removing at least 45% of the anthropogenic nutrients inputs added to both basins of the MS between 1950 and 2030, and 3) variations in intermediate and deep water formation rates that add high natural noise to the P and N concentration trajectories.

ACRONYMS

ASW – Atlantic Surface Water
BiOS – Bimodal Oscillation System
DON – dissolved organic nitrogen
DOP – dissolved organic phosphorus
DW – deep water
EMDW – Eastern Mediterranean Deep Water
EMIW – Eastern Mediterranean Intermediate Water
EMS – Eastern Mediterranean Sea
EMSW – Eastern Mediterranean Surface Water
EMT – Eastern Mediterranean Transient
IW – intermediate water
LIW – Levantine Intermediate Water
MS – Mediterranean Sea
N - nitrogen
NH_4 – dissolved ammonium
NO_3 – dissolved nitrate plus nitrite
NWM – North West Mediterranean
P - phosphorus
PDF – probability distribution function
PO_4 – dissolved phosphate
PON – particulate organic nitrogen
POP – particulate organic phosphorus
SGD – submarine groundwater discharge
SW – surface water
THC – thermohaline circulation
WMDW – Western Mediterranean Deep Water
WMIW – Western Mediterranean Intermediate Water
WMS – Western Mediterranean Sea
WMSW – Western Mediterranean Surface Water
WMT – Western Mediterranean Transition

1 INTRODUCTION

Since the industrial revolution, anthropogenic emissions of phosphorus (P) and nitrogen (N) have rapidly increased worldwide (Galloway, 2014; Cordell et al., 2011; Mackenzie et al., 2011), causing widespread changes in the structure, functioning and health of aquatic ecosystems. Anthropogenic inputs of reactive N to the environment have risen roughly nine-fold since 1860, with a large exponential increase since 1950 (Galloway, 2014). The resulting N load to the oceans has approximately doubled (Galloway, 2014), while P fluxes to the global ocean are 1.5 to three times greater than estimates for pre-anthropogenic times (Ruttenberg, 2014; Paytan and McLaughlin, 2007; Follmi, 1996). Impacts are particularly severe in semi-enclosed seas such as the Baltic and Black Seas where primary production has increased by factors of four to six in recent decades (Mikaelyan et al., 2013; Gustafsson et al., 2012).

Given its large, and growing, coastal population, and the ongoing agricultural and industrial intensification (Micheli et al., 2013; UNEP/MAP, 2012), one may expect widespread evidence of nutrient enrichment in the semi-enclosed Mediterranean Sea (MS). For comparison, land-derived inputs of P and N to the Eastern Mediterranean Sea (EMS) per unit surface area are similar to those entering the Baltic Sea (Van Cappellen et al., 2014). However, despite the high anthropogenic inputs, the MS shows little evidence of increased eutrophication, with the exception of nearshore areas, such as the northern Adriatic Sea, the Gulf of Lions, and the Nile delta region (Karydis and Kitsiou, 2012). The anti-estuarine circulation of the MS and the resulting lateral export of nutrient P and N, ultimately to the North Atlantic Ocean, are usually invoked to explain why the MS remains in its oligotrophic state (Krom et al., 2010; Crispi et al., 2001).

The intermediate (IW) and deep (DW) waters of the Western Mediterranean Sea (WMS) and EMS have relatively short residence times (7-150 years; Powley et al., 2016a; Roether and Well, 2001; Stratford et al., 1998; Béthoux and Gentili, 1996; Roether and Schlitzer, 1991). Hence, the dissolved P and N concentrations of these reservoirs could potentially record anthropogenic nutrient enrichment on a decadal time scale. However, although DW temperature and salinity data for the WMS have been systematically increasing since the early 20th century (0.3-5x10^{-3} ^{o}C yr^{-1} and 0.6-2.2 x10^{-3} PSU yr^{-1}; Marty and Chiaverini, 2010 and references therein), the temporal trends of dissolved nutrient concentrations in the IW and DW of the MS are far more uncertain (Karafistan et al., 2002; Béthoux et al., 1998; Denis-Karafistan et al., 1998). For example, Pasqueron de Fommervault et al. (2015) recently reported evidence for increasing dissolved nitrate (NO_3) concentrations between 1990 and 2010 at the DYFAMED site, a permanent mooring station located in the Ligurian Sea, but at the same time they found that the dissolved phosphate (PO_4) concentrations were decreasing.

One major difficulty in interpreting temporal trends in water column P and N concentrations is the natural variability of the thermohaline circulation (THC). A well-known example is the Eastern Mediterranean Transient (EMT), when DW supply from the Aegean Sea rose markedly above background values for a period of about ten years (Roether et al., 2007). The changes in properties of IW entering the WMS from the EMS through the Strait of Sicily subsequently led to changes in DW formation within the WMS, termed the Western Mediterranean Transition, or WMT (Schroeder et al., 2006). The average DW formation rate in the WMS during the WMT was several times higher than in pre-WMT times (Powley et al., 2016a).

The EMT has recently been proposed to be a manifestation of a bimodal oscillation system (BiOS) in the northern Ionian Sea and the southern Adriatic Sea whereby the North Ionian Gyre switches from anticyclonic to cyclonic on a decadal time scale (Gačić et al., 2010; Pinardi et al., 2015; Malanotte-Rizzoli et al., 1999). BiOS profoundly changes the physical and chemical properties of water masses in the southern Adriatic Sea, as well as those of surface water (SW) that just entered the EMS through the Strait of Sicily and IW entering the Levantine Sea from the Ionian Sea (Civitarese et al., 2010; Gačić et al., 2010). In addition to these relatively long-term variations in circulation regime, the THC of the MS also demonstrates significant inter-annual variability (Pinardi et al., 2015; Sevault et al., 2014; L'Hévéder et al., 2013; Vervatis et al., 2013).

Variations in THC affect the spatial distributions of P and N and can, thus, be a source of variability in time series concentrations measured at given locations in the MS. As an example, changes in PO_4 and NO_3 concentrations in Levantine Intermediate Water (LIW) collected off the coast of Israel appear to coincide with changes in circulation due to BiOS (Ozer et al., 2016). Ozer et al. (2016) therefore propose that the observed changes in the dissolved inorganic nutrient concentrations can be explained by variations in circulation driven by BiOS. In contrast, Moon et al. (2016) argue that the temporal trends exhibited by the concentrations of PO_4 and NO_3 in IW across the whole MS are driven by changes in anthropogenic inputs of P and N, mainly from rivers for P and atmospheric deposition for N. These opposing views raise the question whether time series P and N concentration data of offshore (or pelagic) waters of the MS can yield records of anthropogenic nutrient enrichment, or not.

The purpose of this study is to evaluate to what extent the trends in dissolved P and N concentrations due to changes in the delivery of anthropogenic nutrients to the MS may be masked by the natural variability in THC. To that end, we first estimate the external reactive P and N inputs to the WMS and EMS between 1950 and 2030. Next, we impose these inputs to an existing coupled P and N mass balance model for the MS (Powley et al., 2017), while at the same time considering a number of different water circulation regimes. For the latter, we consider IW and DW formation rates that either remain constant, change randomly from year to year, or follow historical trajectories reconstructed from literature data. The results are used to assess how sensitive temporal trends in aqueous P and N concentrations, N:P ratios and annual primary production in the WMS and EMS are to human-driven changes in land-derived nutrient inputs. Based on our analysis of the modeling results, we formulate recommendations that should help enhance the efficiency of monitoring programs aimed at assessing the impacts of anthropogenic pressures on the biogeochemical state of the MS.

2 METHODS

This paper builds on our previous modeling work on the coupled P and N cycling, first in the EMS (Powley et al., 2014; Van Cappellen et al., 2014), and subsequently extended to include the WMS (Powley et al., 2016a, 2017). The reader is referred to these earlier publications for in-depth presentations of methods, approaches and data sources.

2.1 Mass balance model

The model framework used in this study (Figure 1) is the same as in Powley et al. (2017). The water columns of the WMS and EMS are divided into three horizontal layers: surface water (WMSW, EMSW), intermediate water (WMIW, EMIW) and deep water (WMDW, EMDW). The WMS and EMS models are coupled by the bidirectional water exchanges through the Strait of Sicily. The WMS receives SW inflow from the Atlantic Ocean, while WMIW and WMDW flow back to the Atlantic Ocean. Note that the areas of DW formation in the WMS and EMS are not explicitly included in the model domain; instead the corresponding DW formation fluxes are imposed as boundary fluxes within the model. For the WMS, DW formation occurs in the area of open ocean convection located near to the Gulf of Lions in the northwest Mediterranean and, henceforth, referred to as NWM. For the EMS, DW formation originates in the Adriatic and Aegean Seas. The surface areas of the WMS and EMS model domains (i.e., excluding the DW formation areas) are 815×10^3 and 1336×10^3 km^2, respectively.

The model considers three reactive P and four reactive N pools in each horizontal water layer: dissolved inorganic phosphate (PO_4), particulate organic phosphorus (POP), dissolved organic phosphorus (DOP), dissolved nitrate plus nitrite (NO_3), particulate organic nitrogen (PON), dissolved organic nitrogen (DON), and dissolved ammonium (NH_4). The total reactive P input to the model domain equals the sum of PO_4, POP and DOP inputs, plus the fraction of inorganic particulate phosphorus input that becomes soluble after entering the MS (Van Cappellen et al., 2014). The total reactive N input is the sum of NO_3, PON, DON and NH_4 inputs.

Internal cycling of P and N within each water layer is modeled using simple first order (or linear) kinetics. Linear expressions are also applied to the denitrification flux, and the sinking and burial POP and PON fluxes. Each rate constant (k) is calculated from the initial source reservoir mass and output flux in the 1950 steady state model. The exception is assimilation of NO_3 in the SW reservoirs. The average annual primary production in both WMS and EMS is assumed to be P limited (Powley et al., 2017). Nitrogen limitation may occur during parts of the year and in certain localities, especially in the WMS. However, on an annual basis, P limitation drives basin-wide primary productivity across the MS (Lazzari et al., 2016). In the model, the P and N cycles are therefore assumed to be coupled via the Redfield ratio, that is, N assimilation is computed from the P assimilation flux using a 16:1 molar ratio (Redfield et al., 1963). Similarly, carbon fixation during primary production is calculated from the P assimilation flux assuming a Redfield C:P ratio of 106:1.

Fluxes of the various reactive P and N species between water reservoirs are calculated by multiplying the corresponding water flows with the species concentrations in the source reservoirs. The turbulent mixing fluxes are the exception: they are computed by multiplying the difference in concentration between receiving and source reservoirs with an exchange coefficient, where the latter is related to the turbulent diffusion coefficient (Van Cappellen et al., 2014). During the simulations, the concentrations of the various P and N species in the water reservoirs change from year to year. The nutrient fluxes within the MS domain may therefore change over time because of changes in concentrations, changes in water flows, or both.

Overall, the model consists of 42 ordinary differential equations solved in MATLAB using solver ODE 15s. Factorial design sensitivity analyses performed by Powley et al. (2017) indicate that primary productivity and the NO_3:PO_4 ratios within both the WMS and EMS are most sensitive to changes in the fluxes of P and N entering the MS from the North Atlantic Ocean, and changes in the atmospheric deposition fluxes of PO_4 and DON. Furthermore, the EMDW NO_3:PO_4 ratio was found to be more sensitive to processes taking place in the WMS rather than the EMS.

2.2 Reactive phosphorus and nitrogen inputs: 1950 to 2030

The model considers the following sources of reactive P and N to the WMS and EMS: inflows from adjacent marine basins, atmospheric deposition, N_2 fixation, riverine inputs, submarine groundwater discharge (SGD) and direct domestic wastewater discharges. Powley et al. (2017) estimated the magnitudes of these inputs in 1950, that is, before the large increases in anthropogenic P and N emissions that occurred in subsequent decades. These estimates indicated that the inflow of Atlantic Surface Water (ASW) via the Strait of Gibraltar represents the largest input of reactive P and N to the MS. Because our focus is on the detection of anthropogenic signatures in temporal trends of P and N concentrations within the MS, the supply fluxes of reactive P and N associated with ASW inflow are assumed to remain constant over the period 1950-2030. This validity of this assumption is difficult to ascertain given the scarcity of data available to constrain the temporal variability of P and N fluxes through the Strait of Gibraltar. Thus, all the variations in reactive P and N inputs to the MS since 1950 imposed in the model calculations are of anthropogenic origin.

Anthropogenic forcing functions for the individual reactive P and N inputs to the WMS and EMS from 1950 to 2030 are derived following Powley et al. (2014). The values of the reactive P and N inputs in 1950 of Powley et al. (2017) are used as baseline values. For each input, the forcing function then provides for any given year during the 1950-2030 period the change in input flux relative to that in 1950. Thus, a forcing function value of 1.2 in 1994 means the corresponding annual input in 1994 is 20% larger than in 1950. Powley et al. (2014) provide a detailed account of the forcing functions for anthropogenic P and N inputs to the EMS for the period 1950-2000. Table 1 summarizes how forcing functions for both WMS and EMS, and for the entire 1950-2030 period, are obtained; full details are given in the Supplementary Material. Because direct measurements that constrain the temporal evolution of reactive P and N inputs to the MS are quite limited, relatively large uncertainties are associated with the estimated forcing functions. This is particularly true for the 2000-2030 period, where the forcing functions depend on projections of ongoing trends of anthropogenic drivers into the future, for example, the growth of coastal populations and upgrades to wastewater treatment plants in the various countries surrounding the MS. Therefore, for 2000 to 2030, mean values of the forcing functions are given, as well as estimates of upper and lower limits of the associated anthropogenic drivers. Figure S1 shows the anthropogenic forcing functions applied to the model as a function of time. The total anthropogenic forcing functions for the WMS and EMS are displayed in Figure 2.

In addition to the input fluxes described in Table 1, the fluxes of P and N to the DW of the WMS and EMS supplied by DW formation also vary over time, because of 1) the changes in the amounts of P and N carried by the IW and SW that enter the region of DW formation where they mix to form the new DW, and 2) the changes in the nutrients added directly to the DW formation sites via rivers and atmospheric deposition. Here, we derive the forcing functions for the anthropogenic P and N added to each formation site. Changes in the reactive P and N delivered to the DW formation sites from the SW and IW reservoirs are automatically accounted for as the nutrient concentrations in these reservoirs are updated by the model at each time step. Riverine fluxes into the Adriatic Sea and Aegean Sea over the 1950-2030 period are those estimated by Ludwig et al. (2009, 2010). The DON flux entering the Aegean Sea through the Bosphorus is assumed to change proportionally to the reactive N riverine input to the Black Sea (Ludwig et al., 2009, Ludwig et al., 2010). Inflow through the Bosphorus is assumed to be a negligible source of inorganic N and P to the Aegean Sea (Krom et al., 2004). Note that riverine fluxes of reactive P and N are not included for the NWM domain because it corresponds to an area of open ocean convection and thus lacks a coastline. Atmospheric deposition fluxes of P and N to the Adriatic Sea, Aegean Sea and NWM are assumed to follow the same historical trends of those of the entire EMS and WMS.

2.3 Thermohaline circulation (THC)

This study focuses on the inter-annual variability in THC and, more specifically, the year-to-year changes in the rates of IW and DW formation originating from the four main source zones in the MS: the NWM for the WMS, and the Rhodes Gyre, Adriatic Sea and Aegean Sea for the EMS. During any given year, the IW/DW formation rates remain constant. Four different scenarios are considered to illustrate the sensitivity of the P and N distributions to circulation (Table 2): 1) time-invariant circulation, 2) random fluctuating IW/DW formation rates, 3) reconstructed (historical) IW/DW formation rates, and 4) attenuated historical IW/DW formation rates. Each circulation scenario is run separately from, and together with, the 1950 to 2030 reactive P and N inputs (Table 2) to separate the contributions of THC from those associated with anthropogenic nutrient enrichment. The observables targeted by our analysis are the reactive P and N concentrations in the IW and DW reservoirs, the corresponding N:P ratios, and primary productivity. Once the prescribed IW/DW formation flows are imposed, the other water fluxes are adjusted to maintain the annual water balance of each reservoir included in the model. The total inflow and outflow water fluxes through the Strait of Gibraltar are kept constant in all model runs, although the proportions of WMIW and WMDW in the outflow to the Atlantic Ocean vary over time. Note that water fluxes between WMSW and WMIW, and WMIW and WMDW, may change direction during some of the model simulations.

2.3.1 Random circulation 1950-2030 (Simulations 1 and 2)

A random normal or lognormal probability distribution function (PDF) is used to generate yearly IW/DW formation rates from each source region between 1950 and 2030 (Table 3). The PDFs are based on modeled IW/DW formation rates in the four regions: DW formation in the NWM has been reported to occur in 53% of years over the period 1959-2001 (L'Hévéder et al., 2013), 63% of years in the Aegean Sea over the period 1961-2000 (Vervatis et al., 2013), 80% of years in the Adriatic Sea over the period 1987-2007 (Pinardi et al., 2015), while EMIW formation (also termed LIW in the literature) occurs every year (Vervatis et al., 2013). Mean values and standard deviations of IW/DW formation flows are assigned using long term model estimates from the literature, normalized so that the long term mean value of any given IW/DW formation rate equals the value used in the 1950 steady state water cycle of Powley et al. (2016a). The corresponding THC parameter values are given in Table 3. The variability in P and N concentrations due to random fluctuations in THC are assessed by carrying out 500 model runs with randomly selected values of the IW/DW formation rates. Mean, 10th and 90th percentile concentrations are reported (see below).

2.3.2 Reconstructed (historical) circulation 1960-2000 (Simulations 4 and 5)

Estimates of historical IW/DW formation rates between 1960 and 2000 are obtained from the yearly rates of EMIW (or LIW) and Aegean DW formation reported by Vervatis et al. (2013), and WMDW formation in the NWM by L'Hévéder et al. (2013), normalized as in section 2.3.1 so that the long term mean value of any given IW/DW formation rate equals the steady state value used in the 1950 water cycle of Powley et al. (2016a). The resulting DW and IW formation rates exhibit large year-to-year variations (Figure S3). In particular, intense WMDW formation rates during the first half of the 1980s is followed by a period of relatively little WMDW formation extending into the 1990s.

Because of the lack in the literature of long term predictions for DW formation in the Adriatic Sea before 1980, we assume that the corresponding DW formation flow follows the observed salinity cycle in the Adriatic Sea due to BiOS (Civitarese et al., 2010). The changes in salinity in the Adriatic Sea caused by BiOS alter the density of Adriatic water and therefore influence the rate of DW formation. To simulate the BiOS driven changes in Adriatic DW formation the following sine wave is used:

$$y(t) = (Asin(\omega t + \varphi) + 1) \,.\, 1950_{water}^{Adr} \quad (1)$$

where A is the amplitude, ω the frequency, and φ the phase shift of the DW flow out of the Adriatic Sea, and 1950_{water}^{Adr} the 1950 flow (0.32 Sv); A is assigned the value of 0.98 Sv based on the reported range of Adriatic DW flow into the EMS (0.006-0.63 Sv; Pinardi et al., 2015; Sevault et al., 2014), ω is assigned a value of $\pi/8$ to represent a period of 16 years, matching that of salinity variations in the south Adriatic Sea (Civitarese et al., 2010), and φ is equal to 0.7 so that the greatest (smallest) DW formation rate occurs at the highest (lowest) observed salinity. We further discretize the sine wave so that the DW formation rate remains constant throughout a given year to be consistent with the formulations used for the other IW/DW formation sites. The sine wave produced by Equation 1 and the resulting Adriatic DW formation rates are shown in Figures S2 and S3, respectively.

2.3.3 Attenuated historical IW/DW formation rates (Simulations 6 and 7)

The mass balance calculations assume that the water fluxes across the entire MS instantaneously adjust to changes in IW and DW formation rates, which is admittedly an oversimplification of the true circulation dynamics inherent to the box modeling approach followed in this study. To relax this assumption and account for attenuation and delays in the propagation of changes in water fluxes, a running average of the previous 5 year IW/DW formation rates is computed and applied to the model for each formation site across the MS. Note that while the 5-year averaging is arbitrary, it is selected to be of similar magnitude as the SW and IW water residence times. Similar to the previous circulation scenarios, resulting changes in the water fluxes throughout the rest of the model are continuously adjusted to maintain the water balance.

3 RESULTS

3.1 Reactive phosphorus and nitrogen inputs: 1950-2030

For the WMS, our estimates indicate that the reactive P input from land derived sources increases by a maximum factor of three relative to the 1950 input, reaching a peak in the 1980s (Figure 2). However, because of the dominance of marine derived inputs in the nutrient budgets of the MS, the total reactive P input to the WMS only increases by a maximum of 16% between 1950 and 2030, from 13.4 x 10^9 mol P yr^{-1} in 1950 to a maximum of 15.6 x 10^9 mol P yr^{-1} in 1985, largely driven by the increase in riverine supply of PO_4 (Figure 3A). A subsequent decline in the reactive P input occurs until the year 2008 after which it slowly rises again to 14.8 x 10^9 mol yr^{-1} by 2030, because of the increasing inputs from riverine and wastewater sources as a result of rapid coastal population growth.

For the EMS, the reactive P input from land derived sources increases by a maximum factor of 2.3 (Figure 2). The maximum increase of the total reactive P input is 39%, from 5.6 x 10^9 mol yr^{-1} in 1950 to 7.8 x 10^9 mol yr^{-1} in 1984, mainly as a result of increased atmospheric deposition, riverine input and DW inflow from the Adriatic Sea (Figure 3B). Similar to the WMS, the reactive P input to the EMS then decreases until 2000 before increasing by an additional 0.4 x 10^9 mol yr^{-1} between 2000 and 2030. From 1950 to 2030, most of the reactive P entering the WMS and EMS is associated with inflow through the Straits of Gibraltar and Sicily. The marine derived sources account for 85-94% of the total reactive P input to the WMS, and 62-77% to the EMS. The larger fraction of reactive P from non-marine sources explains why the relative changes in total reactive P input to the EMS are larger than for the WMS.

In contrast to P, the reactive N inputs to the WMS and EMS are predicted to continually increase between 1950 and 2030 (Figure 3 C and D). By 2030, the land derived reactive N inputs are 3 and 2.5 times higher than in 1950 for the WMS and EMS, respectively (Figure 2). In the WMS, the total reactive N input increases by 51%, from 398 x 10^9 mol yr^{-1} in 1950 to 599 x 10^9 mol yr^{-1} in 2030 (Figure 3C). As for P, the relative increase in the total reactive N input is greater for the EMS: between 1950 and 2030 it increases by 98%, from 208 x 10^9 mol yr^{-1} to 412 x 10^9 mol yr^{-1} (Figure 3D).

Over the 1950-2030 period, inflow through the Straits of Gibraltar and Sicily provides 79 to 87% of the total reactive N input to the WMS; for the EMS, inflow through the Strait of Sicily supplies 48 to 63% of the total reactive N input. Nitrogen fixation, which had been hypothesized to have a significant impact on DW NO_3:PO_4 ratios of the MS (Béthoux et al., 1992, Béthoux et al. 2002), only accounts for up to 3% of the total reactive N input to the WMS between 1950 and 2030. Submarine groundwater discharge of dissolved reactive N, which is included here for the first time in a dynamic nutrient budget of the MS, becomes increasingly important during the 1950-2030 period, contributing up to 5% of the total reactive N inputs to the WMS and EMS in 2030 compared to only 1% in 1950. Our minimum estimates for the 21st century indicate that the reactive N input may stabilize in the WMS after 2000, and even decrease after 2020 in the EMS. The maximum projections have the total reactive N inputs increase approximately linearly from 2000 to 2030.

3.2 Dissolved reactive phosphorus and nitrogen concentrations

3.2.1 Noise from inter-annual THC variability (Simulations 1 and 2)

The areas shaded in red on Figures 4 and 5 encompass the ranges of dissolved reactive P and N concentrations in the water column generated by random changes in inter-annual THC (Simulation 1). Note that we present only results for the IW and DW reservoirs because nutrient concentrations across the photic zone are spatially and temporally extremely variable, making a comparison between long-term model-predicted SW concentrations and near-sea surface observations tenuous. In Simulation 1, PO_4 and NO_3 concentrations in WMIW and EMIW exhibit the highest absolute sensitivity to inter-annual variations in THC. For the PO_4 concentrations, the mean difference between the 10th and 90th percentiles in WMIW and EMIW over the course of 1950 to 2030 is 34 nM (±6% of the mean 1950-2030 value) and 10 nM (± 5% of mean 1950-2030 value), respectively. For the NO_3 concentrations, the difference is 0.7μM (± 5% of mean 1950-2030 value) in WMIW, and 0.3 μM (± 6% of mean 1950-2030 value) in EMIW.

The PO_4 and NO_3 concentrations of the DW reservoirs are more sensitive to THC changes in the WMS than EMS. The mean differences between the 10th and 90th percentiles of the PO_4 and NO_3 concentrations of WMDW are 27 nM (± 4% of mean value) and 0.6 μM (± 4% of mean 1950-2030 value), respectively, but only 3 nM (±1% of mean 1950-2030 value) and 0.1µM (±1% of mean 1950-2030 value) for the corresponding concentrations in EMDW. Similar to their inorganic counterparts, the highest absolute sensitivities to THC of DOP and DON concentrations are found for the IW reservoirs: 6 nM (± 7% of mean 1950-2030 value) and 0.3 µM (± 5% of mean 1950-2030 value) for DOP and DON, respectively, in WMIW, and 4 nM (± 5% of mean 1950-2030 value) and 0.2 µM (± 3% of mean 1950-2030 value) in EMIW. As expected, for Simulation 2, the variability in concentrations due to the inter-annual variability in THC (blue shaded area; Figures 4 and 5) are of the same order of magnitude as in Simulation 1.

3.2.2 Anthropogenic nutrient enrichment (Simulations 2 and 3)

The temporal trends in the IW dissolved reactive P and N concentrations in Simulation 3 generally reflect those of the P and N inputs to the WMS and EMS over the time period 1950 to 2030 (Figures 3, 4, 5, S4 and S5). Relative to the 1950 baseline, IW dissolved reactive P concentrations increase to a maximum of 13% in the WMS and 21% in the EMS by the late 1980s to early 1990s (Figures 4, 5 and S5), compared to increases in reactive P inputs of 16% and 39% in the WMS and EMS, respectively (Figure 3). Within the DW reservoirs, dissolved reactive P concentrations in both WMS and EMS increase continuously from 1950 to 2030, with the exception of the WMDW DOP concentration, which reaches its maximum in 1993 with an 11% higher value than in 1950. Dissolved reactive N concentrations in both WMS and EMS increase throughout the simulation period reaching their maximum values in 2030 (Figures 4, 5, S4 and S5). In particular IW DON concentrations are predicted to strongly increase by a maximum of 33% in the WMS and 78% in the EMS by 2030 relative to the 1950 concentrations (Figure S5). The NO_3 concentrations in the WMS and EMS increase strongly after the 1980s, with both IW and DW NO_3 concentrations increasing between 2000 and 2030 at almost linear rates of 0.02-0.04 µM yr^{-1} in the WMS and 0.01-0.03 µM yr^{-1} in the EMS (Figures 4 and 5). By 2030, NO_3 concentrations of WMIW are comparable to those of WMDW. The mean dissolved reactive P and N concentrations of Simulation 3 closely match those of Simulation 2 as both simulations use the same anthropogenic forcings.

3.2.3 Reconstructed historical circulation changes (Simulations 4 to 7)

The results of the historical THC changes (1950 to 2000) are shown in Figures 6, S6, S7 and S8. The maximum variations in PO_4 concentrations in Simulation 4 are 75 nM and 29 nM in WMIW and EMIW, respectively, and 33 nM and 4 nM in WMDW and EMDW. For NO_3 concentrations, the maximum variations are 1.6 µM and 0.6 µM in WMIW and EMIW, respectively, and 0.7 µM and 0.1 µM in the WMDW and EMDW. Imposing the 5-year running average of IW/DW historical formation rates (Simulation 6) yields maximum variations in PO_4 and NO_3 concentrations that are 39-53% lower in IW and 16-25% lower in DW than in Simulation 4. Note that the P and N concentration trajectories of Simulations

5 and 7 are shifted upwards from those of Simulation 4 and 6 respectively, because the former include the post-1950 anthropogenic nutrient inputs (Figures 6 and S6).

3.3 N:P ratios

The dissolved organic P and N pools record the greatest change in N:P ratios over the course of the 1950-2030 period, with the largest changes in the EMS (Figure 7; Table S2). In EMIW, the mean molar DON:DOP ratio increases from 67 in 1950 to a maximum of 100 by 2030 as a result of anthropogenic nutrient enrichment. This increase by 49% far exceeds the variability of only 5% caused by random fluctuations in inter-annual THC. Similarly, increases in the mean NO_3:PO_4 ratios of WMIW and EMIW of up to 38% exceed changes due to random variations in THC by more than a factor of five. The DW NO_3:PO_4 ratios of the WMS and EMS show the smallest increases with time, although these are the most frequently reported N:P ratios for the MS. In the WMS, the modeled NO_3:PO_4 DW ratio remains approximately constant at a value 21 until the early 1990s, before increasing approximately linearly to a value of 22.6 by 2030 (see also Figure S9). In EMDW the NO_3:PO_4 ratio slightly decreases from 28.3 in 1950 to a minimum of 28.0 in 1989, as a result of the reduced input from the Nile River after closure of the Aswan Dam, before increasing to 29.5 by 2030. In the historical circulation scenarios, the drop in IW and DW NO_3:PO_4 ratios of the WMS and EMS during the 1980s and their subsequent recovery during the 1990s primarily reflect the variations in the reconstructed THC (Figure S10).

3.4 Primary productivity

According to Simulation 3, the variable inputs of anthropogenic reactive P and N increase primary productivity in the WMS from 148 g C m^{-2} yr^{-1} in 1950 to 166 g C m^{-2} yr^{-1} in 1987 (12% increase), followed by a decrease to 159 g C m^{-2} yr^{-1} by 2011 with little change afterwards (Figure 8). A larger relative increase is seen for the EMS in Simulation 3, with primary productivity rising from 56 g C m^{-2} yr^{-1} in 1950 to 69 g C m^{-2} yr^{-1} in 1989 (22% increase) and settling to a final value of 67 g C m^{-2} yr^{-1} in 2030. The random THC fluctuations in Simulation 1 yield a range in primary productivity in the WMS of around 35 g C m^{-2} yr^{-1} (±12% of mean value), which is nearly twice the maximum change of 18 g C m^{-2} yr^{-1} from the variable inputs of reactive P in Simulation 3. By contrast, for the EMS, the variability produced by random THC (7 g C m^{-2} yr^{-1} or ±6% of the mean value) is smaller than the maximum difference of 13 g C m^{-2} yr^{-1} due to increased anthropogenic reactive P inputs after 1950. The historical THC scenarios (Simulations 4 and 5) yield the largest relative changes in primary productivity in the WMS and EMS, with variations of up to 60% relative to the 1950 values (Figure S11).

4 DISCUSSION

4.1 Phosphorus and nitrogen budgets

The MS is landlocked and experiences high population growth and seasonal tourism along its coastline (Plan-Bleu, 2005). As a result, the MS has seen significant increases in land derived nutrient inputs since 1950 (Powley et al., 2016b, Powley et al., 2014; Ludwig et al., 2009; Guerzoni et al., 1999; this study). Furthermore, the water residence times of the IW and DW reservoirs are relatively short (Figure 1), thus suggesting that anthropogenic nutrient enrichment could potentially be recorded by temporal changes in the reactive P and N concentrations within the IW and DW of the MS. So far, however, long-term trends of P and N concentrations in the deeper water layers of the MS have been inconclusive (Pasqueron de Fommervault et al., 2015; Karafistan et al., 2002; Béthoux et al., 1998; Denis-Karafistan et al., 1998). One key contributing factor is the anti-estuarine circulation of the MS, which buffers the impact of anthropogenic nutrient enrichment on the N and P budgets, and helps explain why offshore waters of the MS have remained oligotrophic, in contrast to, for example, the Baltic Sea.

The anti-estuarine circulation causes large, bidirectional water exchanges across the Straits of Gibraltar and Sicily. Based on our estimates, the nutrient fluxes carried by these water exchanges dominate the reactive P and N inputs to the WMS and EMS (Figure 3; Powley et al., 2017). In other words, the nutrients fluxes between the North Atlantic and the WMS, and between the WMS and EMS, dilute the changes in N and P concentrations induced by the inputs from the surrounding land masses. The latter contribute less than 38% of total reactive P inputs and less than 52% of total reactive N inputs into the WMS and EMS between 1950 and 2030, despite increases in anthropogenic inputs of P and N by factors of 3 (WMS) and 2.5 (EMS) over the same time period (Figure 2). Additionally, the anti-estuarine circulation efficiently removes a large proportion of the excess anthropogenic nutrients. On the order of 45% of the excess reactive P and N added to the EMS between 1950 and 2030 are removed from the EMS via outflow through the Strait of Sicily (Figure 9). Similarly, outflow to the North Atlantic and EMS exports approximately 60% of anthropogenic P and N supplied to the WMS over the same time period.

4.2 Detecting offshore anthropogenic nutrient enrichment

The rates of intermediate and deep-water formation in the WMS and EMS vary significantly from year to year (Pinardi et al., 2015; Sevault et al., 2014; L'Hévéder et al., 2013; Vervatis et al., 2013). This creates noise in the spatial and temporal distributions of biogeochemical properties across the MS, including the concentrations of various forms of P and N, N:P ratios and primary productivity. While our analysis focuses on the impact of inter-annual THC variations on the ability to detect basin-wide temporal trends over decadal time scales, we fully recognize that mesoscale and seasonal variability in circulation may cause additional noise in nutrient enrichment signals. These cannot be accounted for in our simple mass balance calculations and require higher resolution modeling approaches (see, for example, Macias et al., 2014).

According to our results, the detection of changes in the dissolved reactive P concentrations of WMIW and WMDW directly caused by anthropogenic inputs are expected to be hampered by the random noise created by inter-annual variability of THC (Figure 4). The changes in PO_4 and DOP should be more pronounced in EMIW and EMDW (compare Figures 4 and 5). Nonetheless, the predicted maximum increases in the PO_4 and DOP concentrations for the EMS since 1950 are at most of the order of 10 nM, which is close to the analytical precision of 3-5 nM on frozen samples (Pujo-Pay et al., 2011; Krom et al., 2005). Given the sparse measurements of reactive P in the MS, in particular for DOP, together with the analytical limitations, it is unlikely that existing time series PO_4 and DOP data sets can yield unambiguous records of basin-wide anthropogenic nutrient enrichment. Additional practical problems of detecting nutrient changes in the IW is the variable depth of the nutricline, and temporal and spatial variations caused, for example, by mesoscale features.

Temporal changes in NO_3 and DON concentrations should be more readily detectable within time series data. The model generated NO_3 concentrations rise above the background noise of random THC variability in the IW and DW reservoirs of both the WMS and EMS after 1990 (Figures 4 and 5). The largest anthropogenic enrichment signatures are predicted for DON, however. In EMIW, the anthropogenic DON signal is already observed after the 1970s, with an increase in the mean DON concentrations of 2.1 μM between 1950 and 2030. The latter is much greater than the 0.18 μM variation in DON concentrations associated with random THC fluctuations (Figure 5). Likewise, anthropogenic enrichment of DON should be detectable in EMDW and WMIW after 1980 and in WMDW after 1990 (Figures 4 and 5).

The different temporal trends in reactive P and N inputs imply that N:P ratios should be sensitive indicators of anthropogenic nutrient enrichment, with the largest increases predicted for DON:DOP ratios (Figure 7). Reported DON:DOP ratios in the MS tend to be extremely variable, however. They range from 50 to 84, and from 60 to 220, in the photic zone of the WMS and EMS, respectively, and from 67 to 400, and from 25 to 260 in WMDW and EMDW, respectively (Santinelli, 2015). The heterogeneity in reported DON:DOP ratios may largely be due to the difficulty in accurately measuring DOP concentrations, which tend to be very low and require careful blank correction. Our modeling results therefore call not only for a more systematic monitoring of DON and DOP concentrations in the MS, but also for the detailed recording of QA/QC procedures.

Higher than Redfieldian NO_3:PO_4 ratios are a defining feature of the MS: deep water NO_3:PO_4 ratios are probably the most extensively documented feature of nutrient distributions across the WMS and EMS. The existing observational data further show that DW NO_3:PO_4 ratios tend to be more coherent than the DON:DOP ratios; they cluster around 20-23:1 in WMDW and 28:1 in EMDW (Pujo-Pay et al., 2011; Schroeder et al., 2010; Ribera d'Alcalà et al., 2003; Moutin and Raimbault, 2002; Kress and Herut, 2001; Béthoux et al., 1998; Krom et al., 1991). The greater spatial consistency of the DW NO_3:PO_4 ratios are likely due to the higher concentrations of PO_4 in DW (170-400 nM for PO_4 in DW, compared to 25-60 nM for DOP in IW and DW) leading to lower relative errors on the NO_3:PO_4 ratios compared to the DON:DOP ratios. Our mass balance calculations predict that anthropogenic nutrient enrichment should be detectable in the NO_3:PO_4 ratios of WMDW and EMDW after 2000 and 2010, respectively (Figures 7 and S9).

Variations in THC are predicted to cause significant noise in the annual primary production rates of the WMS (Figure 8). A key role of circulation in controlling primary production in the north-west Mediterranean is highlighted by two open ocean convection events that took place in spring 2011: these two events supplied the same amount of PO_4 to the SW as annual riverine discharge and atmospheric deposition together (Severin et al., 2014). In the WMS, DW formation is linked to upwelling of WMIW into WMSW. A similar coupling is absent in the EMS where little upwelling into the SW occurs (Figure 1). This explains why the range of primary productivity associated with random variations in THC is much broader in the WMS than EMS (Figure 8). Overall, our results imply that the relative increase in primary productivity due to anthropogenic nutrient enrichment should be more easily detectable in the EMS than WMS.

The largest driver of the predicted changes in the mean primary productivity of the WMS over the period 1950-2030 is the riverine supply of reactive P input (Figure S12). For the EMS, variations in atmospheric deposition are the main cause of changes in primary productivity until the beginning of the 21st century. By 2030, however, direct wastewater discharges and riverine discharge may catch up with atmospheric deposition as non-marine sources of reactive P to the EMS. Interestingly, the model predicts that riverine inputs to the WMS are as important in controlling primary productivity in the EMS as riverine inputs directly to the EMS, because of the large contribution of inflow of WMSW via the Strait of Sicily to the reactive P budgets of the EMS (Figure 3, see also Powley et al., 2017).

4.3 Historical trajectories

The reconstructed historical changes in THC between 1960 and 2000 significantly affect the distributions of P and N, as well as primary productivity (Figure 6, S6, S7, S8, S10 and S11). The combination of anthropogenic P and N inputs plus historical THC (Simulation 5) yields primary production rates ranging from 125 to 234 g C m^{-2} yr^{-1} in the WMS, and from 55 to 86 g C m^{-2} yr^{-1} in the EMS. These values fall within the observed ranges compiled by Berman-Frank and Rahav (2012) for the period 1970-2009: 37-475 g C m^{-2} yr^{-1} for the WMS and 10-143 g C m^{-2} yr^{-1} for the EMS. Equally important, Berman-Frank and Rahav (2012) did not observe clear temporal trends in time series data on primary productivity in the WMS and EMS between 1970 and 2009, which is consistent with the model predictions (Figure S11). Thus, the noise in primary productivity data due to the relatively large variations in THC masks the effect of excess anthropogenic nutrient inputs on primary production during the last decades of the 20^{th} century.

A comparison of the results of Simulations 3 and 5 implies that time series data on dissolved inorganic P and N concentrations in the WMIW primarily record the impact of variations in THC, while a long-term increasing trend between 1960 and 2000 linked to anthropogenic nutrient enrichment may be inferred for the EMIW (Figure 6). Nevertheless, even for EMIW, the variations in PO_4 and NO_3 resulting from the reconstructed circulation are much greater than those resulting from nutrient enrichment as also proposed by Ozer et al. (2016). Note that all P and N concentrations in the historical simulation scenarios, and indeed all model simulations in this study, are within the range of dissolved reactive P and N concentrations reported across both the WMS and EMS (Table S3).

For WMIW, Moon et al. (2016) recently reported that, between 1990 and 2005, PO_4 and NO_3 concentrations rose on average by 70 nM and 1.98 μM per decade, respectively. For EMIW, the same authors report increases of 50 nM PO_4 and 0.78 μM NO_3 per decade, over the period 1985-2000. They further propose that increasing anthropogenic inputs of PO_4 and NO_3, via riverine discharge and atmospheric deposition, respectively, are responsible for the observed concentration trends. This hypothesis contrasts with our analysis, which suggest that circulation changes mostly modulate the PO_4 and NO_3 trajectories in the IW reservoirs, rather than changing anthropogenic inputs. For example, according to Simulation 3, the maximum increases in PO_4 concentrations of WMIW and EMIW during the 1950-2030 period that can be attributed to nutrient enrichment alone are 27 nM and 17 nM, respectively, that is, much less than the observed decadal increases.

When historical changes in THC are accounted for, however, the model-derived trajectories are consistent with the observed PO_4 and NO_3 concentration changes reported by Moon et al. (2016). In Simulation 5, the PO_4 concentration of WMIW increases by 49 nM between 1990 and 2000, and that of EMIW by 27 nM between 1985 and 2000. Over the same time periods, the increases in NO_3 concentrations are 1.4 μM and 1.0 μM in WMIW and EMIW, respectively (Figure 6). These predicted increases in concentration are of comparable magnitudes as those observed by Moon et al. (2016). Even with attenuated water fluxes

(Simulation 7), the variations in IW PO_4 and NO_3 concentrations during the last decade of the 20th century markedly exceed those due to anthropogenic nutrient inputs alone (Simulation 3). We therefore propose that variations in THC are a major contributor to the observed increases in PO_4 and NO_3 concentrations in the IW reservoirs from 1985 to 2000. This is in line with Ozer et al. (2016) who suggest that temporal trends in observed EMIW NO_3 and PO_4 concentrations are primarily driven by circulation changes.

The lack of substantial change in the predicted DW NO_3:PO_4 ratio of the WMS prior to 1990 (Figure S10) is in agreement with the observations of Béthoux et al. (1998; 2002). Pasqueron de Fommervault et al. (2015) further report an increase by 4.2 units between 1990 and 2010 in the NO_3:PO_4 DW ratio at the DYFAMED station located in the WMS. Although this increase is significantly larger than the corresponding WMS-wide DW increase of the NO_3:PO_4 ratio predicted by our model in both the ensemble and historical simulations, it could reflect DYFAMED's location close to the land-derived nutrient inputs along the northern coast of the WMS.

5 CONCLUSIONS

At first the MS would seem the ideal setting to observe whole-basin impacts of anthropogenic nutrient enrichment: it is almost entirely surrounded by land with a large and rapidly growing coastal population. However, as shown here, several factors complicate the unequivocal detection of anthropogenic signatures in time series P and N concentrations in the offshore waters of the MS. First, marine sources play a dominant role in the P and N budgets of the MS. For the WMS, reactive P and N are overwhelmingly supplied by inflow of ASW through the Strait of Gibraltar and EMIW through the Strait of Sicily. For the EMS, the major reactive source of reactive P and N is WMSW flowing in through the Strait of Sicily, although atmospheric deposition represents a reactive N input of comparable magnitude as the WMSW inflow. Second, the anti-estuarine circulation of the MS efficiently removes a large fraction of newly added nutrients, thus further diluting potential anthropogenic signatures in the temporal and spatial distributions of P and N concentrations. Third, significant variability in IW and DW formation rates introduces noise in time series reactive P and N concentrations. Ignoring the effects of variations in THC therefore greatly increases the possibility of false detection of anthropogenic nutrient enrichment in the water column of the MS.

Over the 1950-2030 period, we estimate that the total reactive P and N inputs to the WMS (EMS) increase by up to 16 (39) and 51 (98) % relative to their 1950 values, respectively. According to our simulation results, however, the accompanying changes in water column PO_4 and DOP concentrations between 1950 and 2030 should hardly be discernible over the background noise created by random inter-annual variability in THC. By contrast, the temporal trajectories of DON concentrations should yield more reliable records of the changes in anthropogenic inputs, especially in the EMS. Within the IW and DW, anthropogenic nutrient enrichment should be detectable in DON time series after around 1970 and 1980 in the EMS and WMS, respectively, assuming that the DON concentration data are acquired using artifact free sampling and storage techniques, and high accuracy analytical methods.

Following from the above, the model calculations predict relatively large changes in the molar DON:DOP ratio with time. Nevertheless, the existing time series data on DON:DOP ratios may not yield reliable records of anthropogenic nutrient inputs because of measurement artifacts. For instance, we predict that between 1950 and 2030 the mean molar DON:DOP ratio in EMIW should increase from 67 to 100, a change exceeding the DON:DOP variability produced by inter-annual THC fluctuations. However, the existing observational data show a very high spatial heterogeneity of DON:DOP ratios across the MS, which we attribute in large part to the difficulties associated with accurately measuring the low concentrations of DOP in the waters of the MS, and, to a lesser extent, those of DON. In comparison, the reported NO_3:PO_4 ratios in the DW of the WMS and EMS are much more consistent, likely because of the much higher quality of dissolved inorganic P and N concentration data compared to their organic counterparts. According to the model calculations, the increases in NO_3:PO_4 DW ratios driven by anthropogenic P and N inputs supplied by land-based sources should be discernable after 2000 in the WMS and after 2010 in the EMS.

The model simulations imply that variations in the annually averaged primary production of the WMS are dominated by the year-to-year variations in DW formation rates rather than by changing anthropogenic nutrient inputs. In the EMS, however, annual primary production should be more sensitive to the changes in nutrient inputs from the surrounding land. These differences between the WMS and EMS are further reflected in the broader ranges of dissolved reactive P and N concentrations produced by inter-annual THC variability in the WMS compared to the EMS. Thus, basin-wide anthropogenic nutrient signals and responses to nutrient enrichment are more likely to be detected in time series data from the EMS than the WMS, provided the data have sufficient spatial and temporal coverage, appropriate sampling and accurate analytical procedures are used, and variations in THC are taken into account.

By unraveling the relative roles of anthropogenic nutrient enrichment and thermohaline circulation in driving inter-annual changes in nutrient distributions of the MS, our mass balance model provides a quantitative framework to (1) hind- and fore-cast nutrient trajectories under changing P and N inputs and THC regimes, (2) interpret existing time series data on reactive P and N concentrations and ratios in the

WMS and EMS, and (3) explain why the trophic state of the MS responds differently to anthropogenic nutrient inputs than other landlocked marine basins, such as the Baltic Sea. Additionally, and equally important, the model results yield practical recommendations for a more effective monitoring of the biogeochemical state of the MS. In particular, we strongly recommend the sustained acquisition of water column P and N data over decadal time periods using appropriate methods that are able to accurately determine the low concentrations of P and N encountered in the offshore water masses of the MS. Furthermore, the monitoring programs should include measurements of DOP and DON, because the concentrations of DON and the DON:DOP ratios are predicted to be among the most sensitive indicators of changing nutrient inputs to the MS (if properly measured!). Especially useful would be time series nutrient data obtained at fixed locations (similar to the DYFAMED site) spread across the entire WMS and EMS. Given the importance of the bidirectional exchanges through the Straits of Gibraltar and Sicily for the reactive P and N budgets, the Straits should be priority locations for systematic nutrient analyses and flow determinations.

6 ACKNOWLEDGEMENTS

We thank Erin Bedford and Zahra Akbarzadeh with help with MATLAB coding. This work was financially supported by the Canada Excellence Research Chair (CERC) Program.

7 REFERENCES

Berman-Frank, I., Rahav, E. (2012). Dinitrogen fixation as a souce for new production inthe Mediterranean Sea: A review, in: Stambler, N. (Ed.), Life in the Mediterranean Sea: A Look at Habitat Changes. Nova Science Publisheres, New York, pp. 199–226.

Béthoux, J.P., Morin, P., Ruiz-Pino, D.P. (2002). Temporal trends in nutrient ratios: chemical evidence of Mediterranean ecosystem changes driven by human activity. Deep. Res. Part II-Topical Stud. Oceanogr. **49**, 2007–2016. doi:10.1016/s0967-0645(02)00024-3

Béthoux, J.P., Morin, P., Chaumery, C., Connan, O., Gentili, B., Ruiz-Pino, D. (1998). Nutrients in the Mediterranean Sea, mass balance and statistical analysis of concentrations with respect to environmental change. Mar. Chem. **63**, 155–169.

Béthoux, J.P., Gentili, B. (1996). The Mediterranean Sea, coastal and deep-sea signatures of climatic and environmental changes. J. Mar. Syst. **7**, 383–394. doi:10.1016/0924-7963(95)00008-9

Béthoux, J.P., Morin, P., Madec, C., Gentili, B. (1992). Phosphorus and nitrogen behavior in the Mediterranean Sea. Deep. Res. Part A-Oceanographic Res. Pap. **39**, 1641–1654.

Civitarese, G., Gačić, M., Lipizer, M., Eusebi Borzelli, G.L. (2010). On the impact of the Bimodal Oscillating System (BiOS) on the biogeochemistry and biology of the Adriatic and Ionian Seas (Eastern Mediterranean). Biogeosciences **7**, 3987–3997. doi:10.5194/bg-7-3987-2010

Cordell, D., Rosemarin, A., Schroder, J.J., Smit, A.L. (2011). Towards global phosphorus security: A systems framework for phosphorus recovery and reuse options. Chemosphere **84**, 747–758. doi:10.1016/j.chemosphere.2011.02.032

Crispi, G., Mosetti, R., Solidoro, C., Crise, A. (2001). Nutrients cycling in Mediterranean basins: the role of the biological pump in the trophic regime. Ecol. Modell. **138**, 101–114. doi:10.1016/s0304-3800(00)00396-3

Denis-Karafistan, A., Martin, J.M., Minas, H., Brasseur, P., Nihoul, J., Denis, C. (1998). Space and seasonal distributions of nitrates in the Mediterranean Sea derived from a variational inverse model. Deep. Res. Part I-Oceanographic Res. Pap. **45**, 387–408. doi:10.1016/s0967-0637(97)00089-7

Erisman, J.W., van Grinsven, H., Grizzetti, B., Bouraoui, F., Powlson, D., Sutton, M.A., Bleeker, A., Reis, S. (2011). The European nitrogen problem in a global perspective, in: Sutton, M.A., Howard, C.M., Erisman, J.W., Billen, G., Bleeker, A., Grennfelt, P., van Grinsven, H., Grizzetti, B. (Eds.), The

European Nitrogen Assessment. Cambridge University Press, Cambridge.

FAOSTAT (2016). Annual Population. URL: http://faostat3.fao.org/download/O/OA/E. Accessed on 13/05/2016

FAOSTAT (2015a). Fertilizer Consumption: Nitrogenous and Phosphate fertilizers. URL: http://faostat3.fao.org/download/R/RA/E. Accessed on 7/05/2016

FAOSTAT (2015b). Emissions Agriculature: Manure Management: Manure N content. URL: http://faostat3.fao.org/download/G1/GM/E. Accessedon 12/05/2016

Follmi, K.B. (1996). The phosphorus cycle, phosphogenesis and marine phosphate-rich deposits. Earth-Science Rev. **40**, 55–124. doi:10.1016/0012-8252(95)00049-6

Gačić, M., Borzelli, G.L.E., Civitarese, G., Cardin, V., Yari, S. (2010). Can internal processes sustain reversals of the ocean upper circulation? The Ionian Sea example. Geophys. Res. Lett. **37**, n/a-n/a. doi:10.1029/2010gl043216

Galloway, J.N. (2014). The Global Nitrogen Cycle, in: Turekian, K.K. (Ed.), Treatise on Geochemistry (Second Edition). Elsevier, Oxford, pp. 475–498. doi:http://dx.doi.org/10.1016/B978-0-08-095975-7.00812-3

Guerzoni, S., Chester, R., Dulac, F., Herut, B., Loye-Pilot, M.D., Measures, C., Migon, C., Molinaroli, E., Moulin, C., Rossini, P., Saydam, C., Soudine, A., Ziveri, P. (1999). The role of atmospheric deposition in the biogeochemistry of the Mediterranean Sea. Prog. Oceanogr. **44**, 147–190.

Gustafsson, B.G., Schenk, F., Blenckner, T., Eilola, K., Meier, H.E.M., Muller-Karulis, B., Neumann, T., Ruoho-Airola, T., Savchuk, O.P., Zorita, E. (2012). Reconstructing the Development of Baltic Sea Eutrophication 1850-2006. Ambio **41**, 534–548. doi:10.1007/s13280-012-0318-x

IPCC (2013). Annex II: Climate System Scenario Tables [Prather, M., G. Flato, P. Friedlingstein, C. Jones, J.-F. Lamarque, H. Liao and P. Rasch (eds.)], in: Stocker, T.F., D. Qin, G.-K. Plattner, M. Tignor, S.K. Allen, J. Boschung, A. Nauels, Y. Xia, Midgley, P.M. (Eds.), Climate Change 2013: The Physical Science Basis. Contribution of Working Group I to the Fifth Assessment Report of the Intergovernmental Panel on Climate Change. Cambridge University Press, Cambridge, United Kingdom and New York, NY, USA.

Karafistan, A., Martin, J.M., Rixen, M., Beckers, J.M. (2002). Space and time distributions of phosphate in the Mediterranean Sea. Deep. Res. Part I-Oceanographic Res. Pap. **49**, 67–82.

Karydis, M., Kitsiou, D. (2012). Eutrophication and environmental policy in the Mediterranean Sea: a review. Environ. Monit. Assess. **184**, 4931–4984. doi:10.1007/s10661-011-2313-2

Kress, N., Herut, B. (2001). Spatial and seasonal evolution of dissolved oxygen and nutrients in the Southern Levantine Basin (Eastern Mediterranean Sea): chemical characterization of the water masses and inferences on the N : P ratios. Deep. Res. Part I-Oceanographic Res. Pap. **48**, 2347–2372.

Krom, M.D., Emeis, K.C., Van Cappellen, P. (2010). Why is the Eastern Mediterranean phosphorus limited? Prog. Oceanogr. **85**, 236–244. doi:10.1016/j.pocean.2010.03.003

Krom, M.D., Woodward, E.M.S., Herut, B., Kress, N., Carbo, P., Mantoura, R.F.C., Spyres, G., Thingstad, T.F., Wassmann, P., Wexels-Riser, C., Kitidis, V., Law, C.S., Zodiatis, G. (2005). Nutrient cycling in the south east Levantine basin of the eastern Mediterranean: Results from a phosphorus starved system. Deep. Res. Part II-Topical Stud. Oceanogr. **52**, 2879–2896. doi:10.1016/j.dsr.2005.08.009

Krom, M.D., Herut, B., Mantoura, R.F.C. (2004). Nutrient budget for the Eastern Mediterranean: Implications for phosphorus limitation. Limnol. Oceanogr. **49**, 1582–1592.

Krom, M.D., Kress, N., Brenner, S., Gordon, L.I. (1991). Phosphorus limitation of primary productivity in the Eastern Mediterranean. Limnol. Oceanogr. **36**, 424–432.

L'Hévéder, B., Li, L., Sevault, F., Somot, S. (2013). Interannual variability of deep convection in the Northwestern Mediterranean simulated with a coupled AORCM. Clim. Dyn. **41**, 937–960. doi:10.1007/s00382-012-1527-5

Lamarque, J.F., Dentener, F., McConnell, J., Ro, C.U., Shaw, M., Vet, R., Bergmann, D., Cameron-Smith, P., Dalsoren, S., Doherty, R., Faluvegi, G., Ghan, S.J., Josse, B., Lee, Y.H., MacKenzie, I.A., Plummer, D., Shindell, D.T., Skeie, R.B., Stevenson, D.S., Strode, S., Zeng, G., Curran, M., Dahl-Jensen, D., Das, S., Fritzsche, D., Nolan, M. (2013). Multi-model mean nitrogen and sulfur deposition from the Atmospheric Chemistry and Climate Model Intercomparison Project (ACCMIP): evaluation of historical and projected future changes. Atmos. Chem. Phys. **13**, 7997–8018. doi:10.5194/acp-13-7997-2013

Lazzari, P., C. Solidoro, S. Salon, and G. Bolzon (2016), Spatial variability of phosphate and nitrate in the Mediterranean Sea: A modeling approach, Deep Sea Res Part I Oceanogr Res Pap, 108, 39-52, doi: 10.1016/j.dsr.2015.12.006

Ludwig, W., Dumont, E., Meybeck, M., Heussner, S. (2009). River discharges of water and nutrients to the Mediterranean and Black Sea: Major drivers for ecosystem changes during past and future decades?

Prog. Oceanogr. **80**, 199–217. doi:10.1016/j.pocean.2009.02.001

Ludwig, W., Bouwman, A.F., Dumont, E., Lespinas, F. (2010). Water and nutrient fluxes from major Mediterranean and Black Sea rivers: Past and future trends and their implications for the basin-scale budgets. Global Biogeochem. Cycles **24**, GB0A13. doi:10.1029/2009gb003594

Macias, D., Garcia-Gorriz, E., Piroddi, C., Stips, A. (2014). Biogeochemical control of marine productivity in the Mediterranean Sea during the last 50 years. Global Biogeochem. Cycles **28**, 897–907. doi:10.1002/2014gb004846

Mackenzie, F.T., De Carlo, E.H., Lerman, A. (2011). Coupled C, N, P, and O Biogeochemical Cycling at the Land–Ocean Interface, in: Treatise on Estuarine and Coastal Science. Academic Press, Waltham, pp. 317–342. doi:http://dx.doi.org/10.1016/B978-0-12-374711-2.00512-X

Malanotte-Rizzoli, P., Manca, B., d'Alcala, M.R., Theocharis, A. (1999). The eastern Mediterranean in the 80's and in the 90's: The big transition emerged from the POEM-BC observational evidence, in: MalanotteRizzoli, P., Eremeev, V.N. (Eds.), Eastern Mediterranean as a Laboratory Basin for the Assessment of Contrasting Ecosystems. pp. 1–6.

Marty, J.C., Chiaverini, J. (2010). Hydrological changes in the Ligurian Sea (NW Mediterranean, DYFAMED site) during 1995-2007 and biogeochemical consequences. Biogeosciences **7**, 2117–2128. doi:10.5194/bg-7-2117-2010

Micheli, F., Halpern, B.S., Walbridge, S., Ciriaco, S., Ferretti, F., Fraschetti, S., Lewison, R., Nykjaer, L., Rosenberg, A.A. (2013). Cumulative Human Impacts on Mediterranean and Black Sea Marine Ecosystems: Assessing Current Pressures and Opportunities. PLoS One **8**. doi:10.1371/journal.pone.0079889

Mikaelyan, A.S., Zatsepin, A.G., Chasovnikov, V.K. (2013). Long-term changes in nutrient supply of phytoplankton growth in the Black Sea. J. Mar. Syst. **117**, 53–64. doi:10.1016/j.jmarsys.2013.02.012

Moon, J.-Y., Lee, K., Tanhua, T., Kress, N., Kim, I.-N. (2016). Temporal nutrient dynamics in the Mediterranean Sea in response to anthropogenic inputs. Geophys. Res. Lett. **43**, 5243–5251. doi:10.1002/2016gl068788

Moutin, T., Raimbault, P. (2002). Primary production, carbon export and nutrients availability in western and eastern Mediterranean Sea in early summer 1996 (MINOS cruise). J. Mar. Syst. **33**, 273–288. doi:10.1016/s0924-7963(02)00062-3

Nenes, A., Krom, M.D., Mihalopoulos, N., Van Cappellen, P., Shi, Z., Bougiatioti, A., Zarmpas, P., Herut,

B. (2011). Atmospheric acidification of mineral aerosols: a source of bioavailable phosphorus for the oceans. Atmos. Chem. Phys. **11**, 6265–6272. doi:10.5194/acp-11-6265-2011

Ozer, T., Gertman, I., Kress, N., Silverman, J., Herut, B. (2016). Interannual thermohaline (1979–2014) and nutrient (2002–2014) dynamics in the Levantine surface and intermediate water masses, SE Mediterranean Sea. Glob. Planet. Change. doi:http://dx.doi.org/10.1016/j.gloplacha.2016.04.001

Pasqueron de Fommervault, O., Migon, C., D′Ortenzio, F., Ribera d'Alcalà, M., Coppola, L. (2015). Temporal variability of nutrient concentrations in the northwestern Mediterranean sea (DYFAMED time-series station). Deep Sea Res. Part I Oceanogr. Res. Pap. **100**, 1–12. doi:http://dx.doi.org/10.1016/j.dsr.2015.02.006

Paytan, A., McLaughlin, K. (2007). The oceanic phosphorus cycle. Chem. Rev. **107**, 563–576. doi:10.1021/cr0503613

Pinardi, N., Zavatarelli, M., Adani, M., Coppini, G., Fratianni, C., Oddo, P., Simoncelli, S., Tonani, M., Lyubartsev, V., Dobricic, S., Bonaduce, A. (2015). Mediterranean Sea large-scale low-frequency ocean variability and water mass formation rates from 1987 to 2007: A retrospective analysis. Prog. Oceanogr. **132**, 318–332. doi:10.1016/j.pocean.2013.11.003

Plan-Bleu (2005). A sustainable future for the Mediterranean: The Blue Plan's Environment and Development Outlook. London, Sterling, VA.

Powley, H.R., Krom, M.D., Van Cappellen, P. (2017). Understanding the unique biogeochemistry of the Mediterranean Sea: Insights from a coupled phosphorus and nitrogen model. Global Biogeochem. Cycles **31**, 1010–1031. doi:10.1002/2017GB005648

Powley, H.R., Krom, M.D., Van Cappellen, P. (2016a). Circulation and oxygen cycling in the Mediterranean Sea: Sensitivity to future climate change. J. Geophys. Res. Ocean. **121**, 8230–8247. doi:10.1002/2016JC012224

Powley, H.R., Dürr, H.H., Lima, A.T., Krom, M.D., Van Cappellen, P. (2016b). Direct Discharges of Domestic Wastewater are a Major Source of Phosphorus and Nitrogen to the Mediterranean Sea. Environ. Sci. Technol. **50**, 8722–8730. doi:10.1021/acs.est.6b01742

Powley, H.R., Krom, M.D., Emeis, K.-C., Van Cappellen, P. (2014). A biogeochemical model for phosphorus and nitrogen cycling in the Eastern Mediterranean Sea (EMS) Part 2. Response of nutrient cycles and primary production to anthropogenic forcing: 1950-2000. J. Mar. Syst. **139**, 420–432. doi:10.1016/j.jmarsys.2014.08.017

Pujo-Pay, M., Conan, P., Oriol, L., Cornet-Barthaux, V., Falco, C., Ghiglione, J.F., Goyet, C., Moutin, T., Prieur, L. (2011). Integrated survey of elemental stoichiometry (C, N, P) from the western to eastern Mediterranean Sea. Biogeosciences **8**, 883–899. doi:10.5194/bg-8-883-2011

Redfield, A.C., Ketchum, B.H., Richards, F.A. (1963). The influence of organisms on the composition of seawater, in: Hill, M.N. (Ed.), The Sea. Interscience, New York, pp. 26–77.

Ribera d'Alcalà, M., Civitarese, G., Conversano, F., Lavezza, R. (2003). Nutrient ratios and fluxes hint at overlooked processes in the Mediterranean Sea. J. Geophys. Res. **108**, 16. doi:8106 10.1029/2002jc001650

Roether, W., Klein, B., Manca, B.B., Theocharis, A., Kioroglou, S. (2007). Transient Eastern Mediterranean deep waters in response to the massive dense-water output of the Aegean Sea in the 1990s. Prog. Oceanogr. **74**, 540–571. doi:10.1016/j.pocean.2007.001

Roether, W., Well, R. (2001). Oxygen consumption in the Eastern Mediterranean. Deep. Res. Part I-Oceanographic Res. Pap. **48**, 1535–1551.

Roether, W., Schlitzer, R. (1991). Eastern Mediterranean deep water renewal on the basis of chlorofluromethane and tritium data. Dyn. Atmos. Ocean. **15**, 333–354.

Ruttenberg, K.C. (2014). The Global Phosphorus Cycle, in: Turekian, K.K. (Ed.), Treatise on Geochemistry (Second Edition). Elsevier, Oxford, pp. 499–558. doi:http://dx.doi.org/10.1016/B978-0-08-095975-7.00813-5

Sandroni, V., Raimbault, P., Migon, C., Garcia, N., Gouze, E. (2007). Dry atmospheric deposition and diazotrophy as sources of new nitrogen to northwestern Mediterranean oligotrophic surface waters. Deep. Res. Part I-Oceanographic Res. Pap. **54**, 1859–1870. doi:10.1016/j.dsr.2007.08.004

Santinelli, C. (2015). DOC in the Mediterranean Sea, in: Hansell, D.A., Carlson, C.A. (Eds.), Biogeochemistry of Marine Dissolved Orgainc Matter. Academic Press, London, UK, pp. 579–608.

Schroeder, K., Gasparini, G.P., Borghini, M., Cerrati, G., Delfanti, R. (2010). Biogeochemical tracers and fluxes in the Western Mediterranean Sea, spring 2005. J. Mar. Syst. **80**, 8–24. doi:10.1016/j.jmarsys.2009.08.002

Schroeder, K., Gasparini, G.P., Tangherlini, M., Astraldi, M. (2006). Deep and intermediate water in the western Mediterranean under the influence of the Eastern Mediterranean Transient. Geophys. Res. Lett. **33**, L21607. doi:10.1029/2006gl027121

Sevault, F., Somot, S., Alias, A., Dubois, C., Lebeaupin-Brossier, C., Nabat, P., Adloff, F., Deque, M., Decharme, B. (2014). A fully coupled Mediterranean regional climate system model: design and evaluation of the ocean component for the 1980-2012 period. Tellus Ser. a-Dynamic Meteorol. Oceanogr. **66**. doi:10.3402/tellusa.v66.23967

Severin, T., Conan, P., de Madron, X.D., Houpert, L., Oliver, M.J., Oriol, L., Caparros, J., Ghiglione, J.F., Pujo-Pay, M. (2014). Impact of open-ocean convection on nutrients, phytoplankton biomass and activity. Deep. Res. Part I-Oceanographic Res. Pap. **94**, 62–71. doi:10.1016/j.dsr.2014.07.015

Stratford, K., Williams, R.G., Drakopoulos, P.G. (1998). Estimating climatological age from a model-derived oxygen-age relationship in the Mediterranean. J. Mar. Syst. **18**, 215–226. doi:10.1016/s0924-7963(98)00013-x

UNEP/MAP (2012). State of Mediterranean Marine and Coastal Environment, UNEP/MAP -Barcelona Convention. Athens.

Van Cappellen, P., Powley, H.R., Emeis, K.-C., Krom, M.D. (2014). A biogeochemical model for phosphorus and nitrogen cycling in the Eastern Mediterranean Sea (EMS). Part 1. Model development, initial conditions and sensitivity analyses. J. Mar. Syst. **139**, 460–471. doi:10.1016/j.jmarsys.2014.08.016

Vervatis, V.D., Sofianos, S.S., Skliris, N., Somot, S., Lascaratos, A., Rixen, M. (2013). Mechanisms controlling the thermohaline circulation pattern variability in the Aegean-Levantine region. A hindcast simulation (1960-2000) with an eddy resolving model. Deep. Res. Part I-Oceanographic Res. Pap. **74**, 82–97. doi:10.1016/j.dsr.2012.12.011

Zekster, I.S., Dzhamalov, R.G., Everett, L.G. (2007). Submarine Groundwater. p466, Taylor and Francis Group, Florida, US.

FIGURE CAPTIONS:

Figure 1: Conceptual model framework. A) Circulation structure and water reservoirs: black arrows represent water fluxes, grey dashed arrows turbulent mixing fluxes. Residence time represents the water residence time in the 1950 steady state model. B) Nutrient model: assimilation of P and N only occur in the surface water (SW) reservoirs and denitrification in the deep water (DW) reservoirs (grey dashed arrows). Abbreviations: NWM = Northwest Mediterranean; assim = assimilation; sol: solubilisation; min: mineralization; nit: nitrification; denit: denitrification. Modified from Powley et al. (2017).

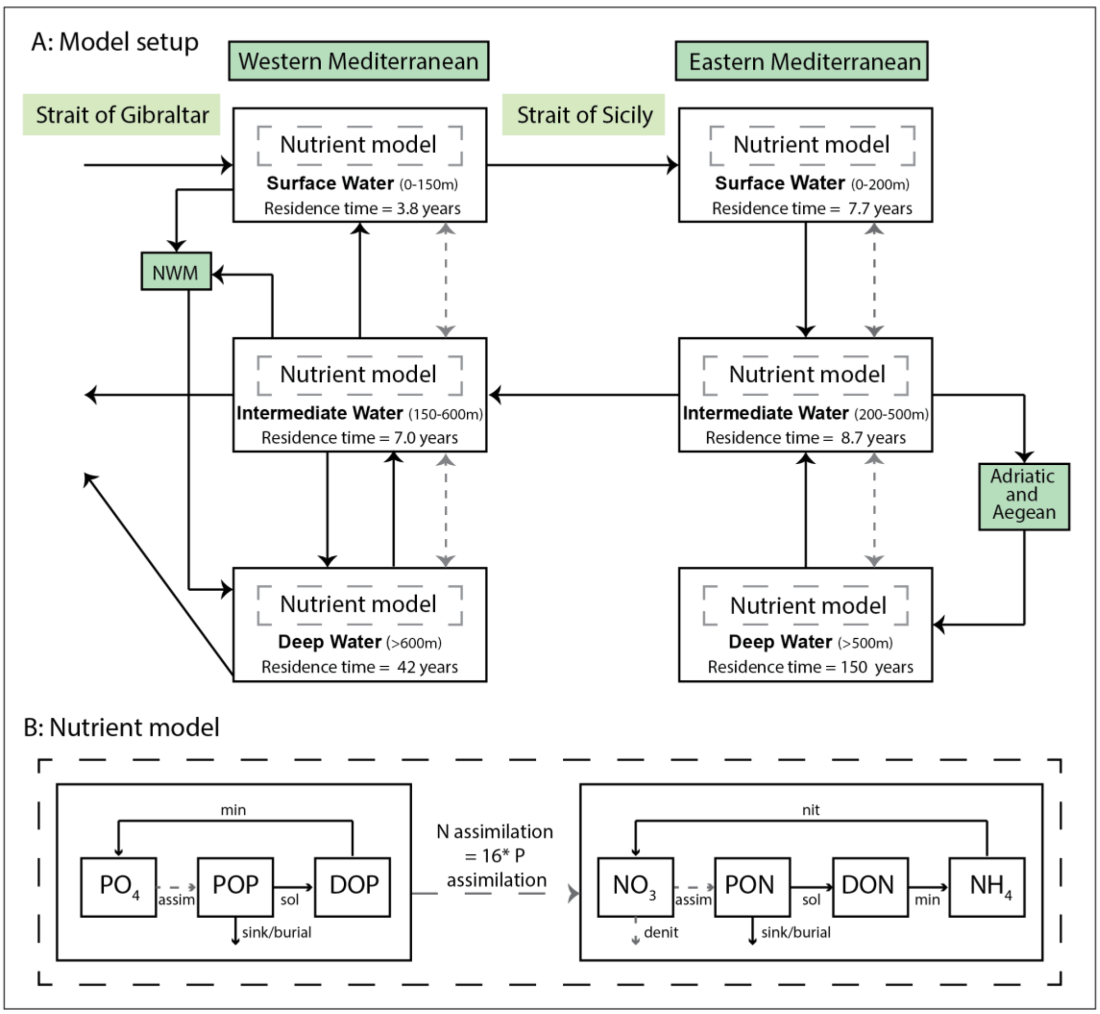

Figure 2: Total anthropogenic forcing functions for phosphorus (black continuous line) and nitrogen (red dashed line) inputs into the WMS and EMS. See text for detailed discussion.

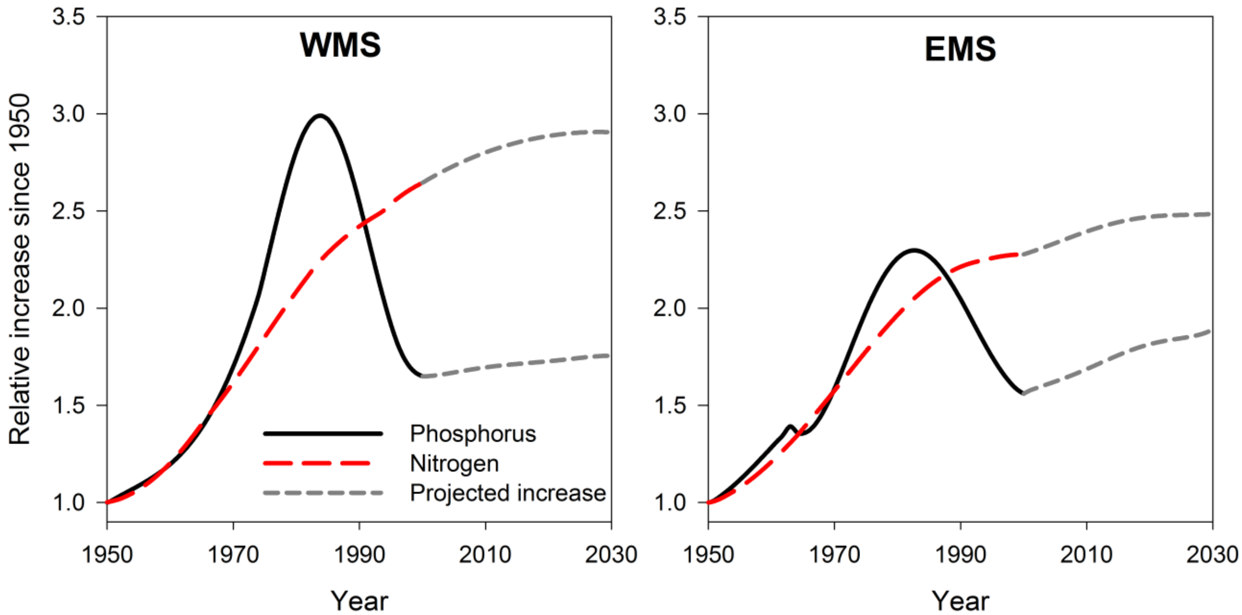

Figure 3: Sources and speciation of reactive phosphorus (A+B) and reactive nitrogen (C+D) inputs into the WMS (A+C) and EMS (B+C) between 1950 and 2030. The changes with time are calculated from the forcing functions described in Table 1, Table S1 and Figure S1, with the exception of the P and N exchanges through the Strait of Sicily. The later are based on the model results of Simulation 3 (constant circulation). Colours refer to the sources of external P and N inputs, hatchings to the chemical speciation of P and N. Pink dashed lines are maximum and minimum estimates of predicted total inputs between 2000 and 2030 (see text for details).

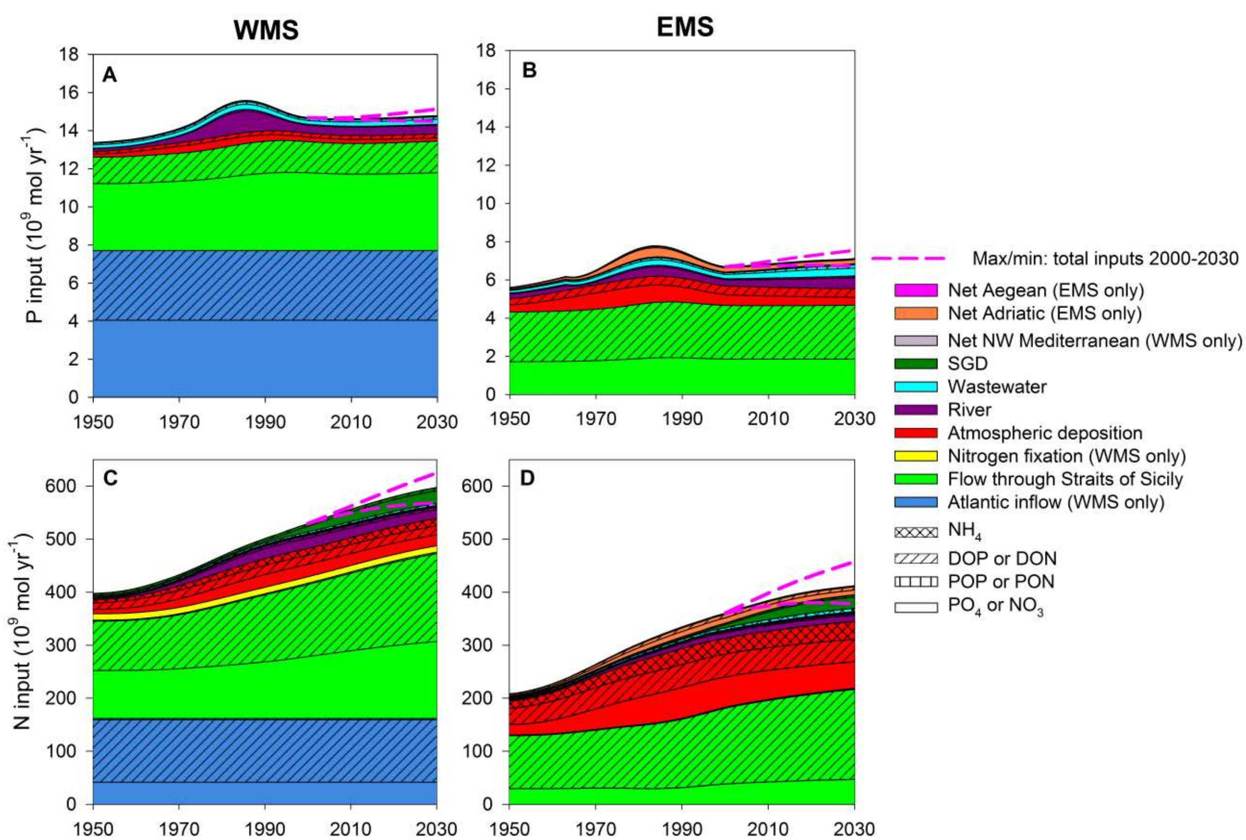

Figure 4: Comparison of 1950-2030 trajectories of intermediate (IW) and deep water (DW) P and N concentrations for the WMS generated by the different scenarios: inter-annual variability of thermohaline circulation (THC) alone (Simulation 1; red shading and red lines), anthropogenic nutrient enrichment plus inter-annual THC variability (Simulation 2; blue shading and blue lines), anthropogenic nutrient enrichment alone (Simulation 3; black line). Mean, 10th and 90th percentiles of 500 model runs are shown. Dashed lines between 2000 and 2030 represent the ranges obtained by considering maximum and minimum estimates of reactive P and N inputs for this time period. Note y-axis changes in scale for different species. See text and Table 2 for details on the model runs. Small discrepancies between the mean concentration trajectories in Simulation 2 and Simulation 3 arise from a change in direction of fluxes between WMIW and WMDW when the flow through the Strait of Sicily drops below 0.53 Sv.

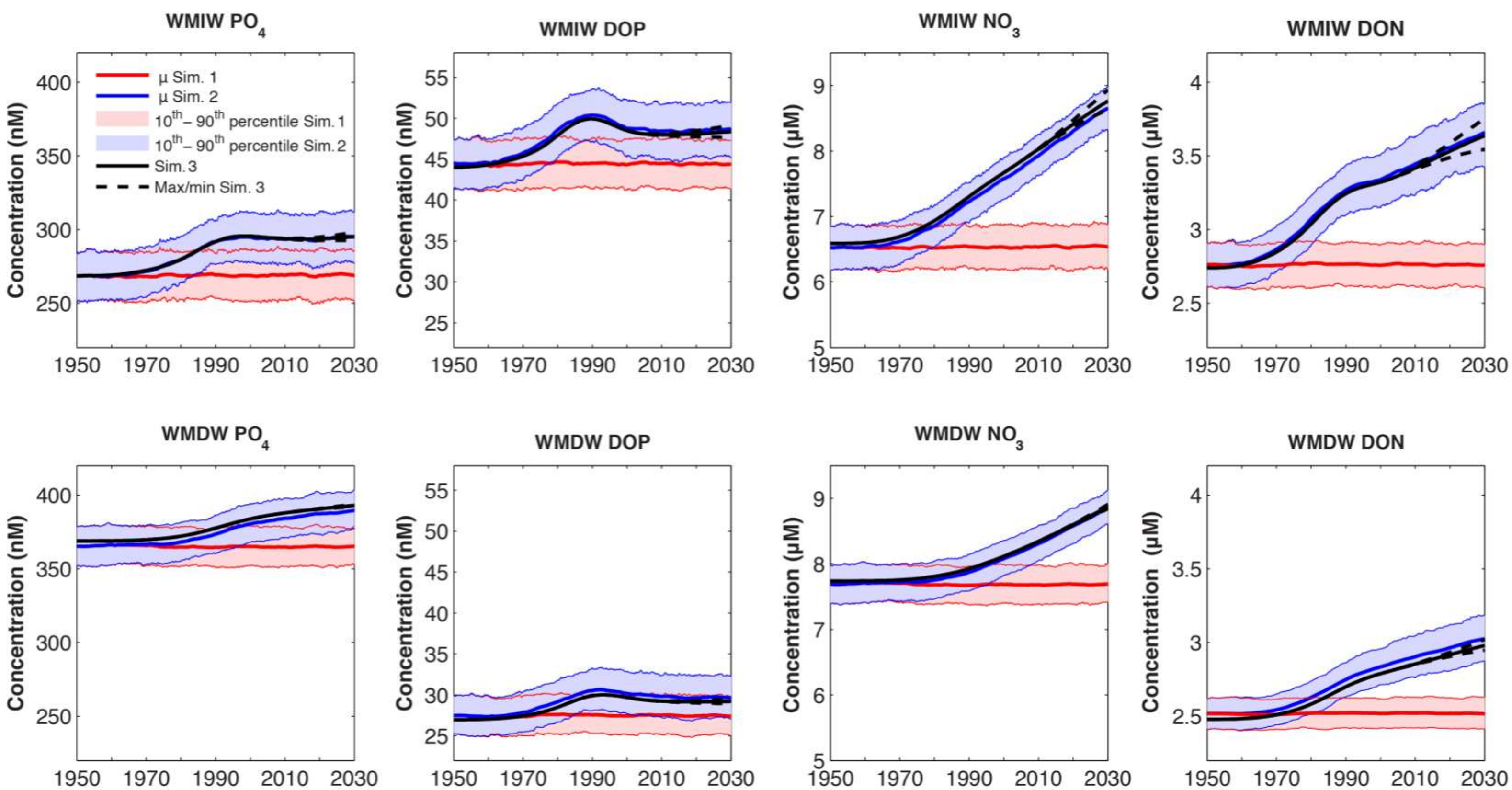

Figure 5: Same as Figure 4 but for the EMS.

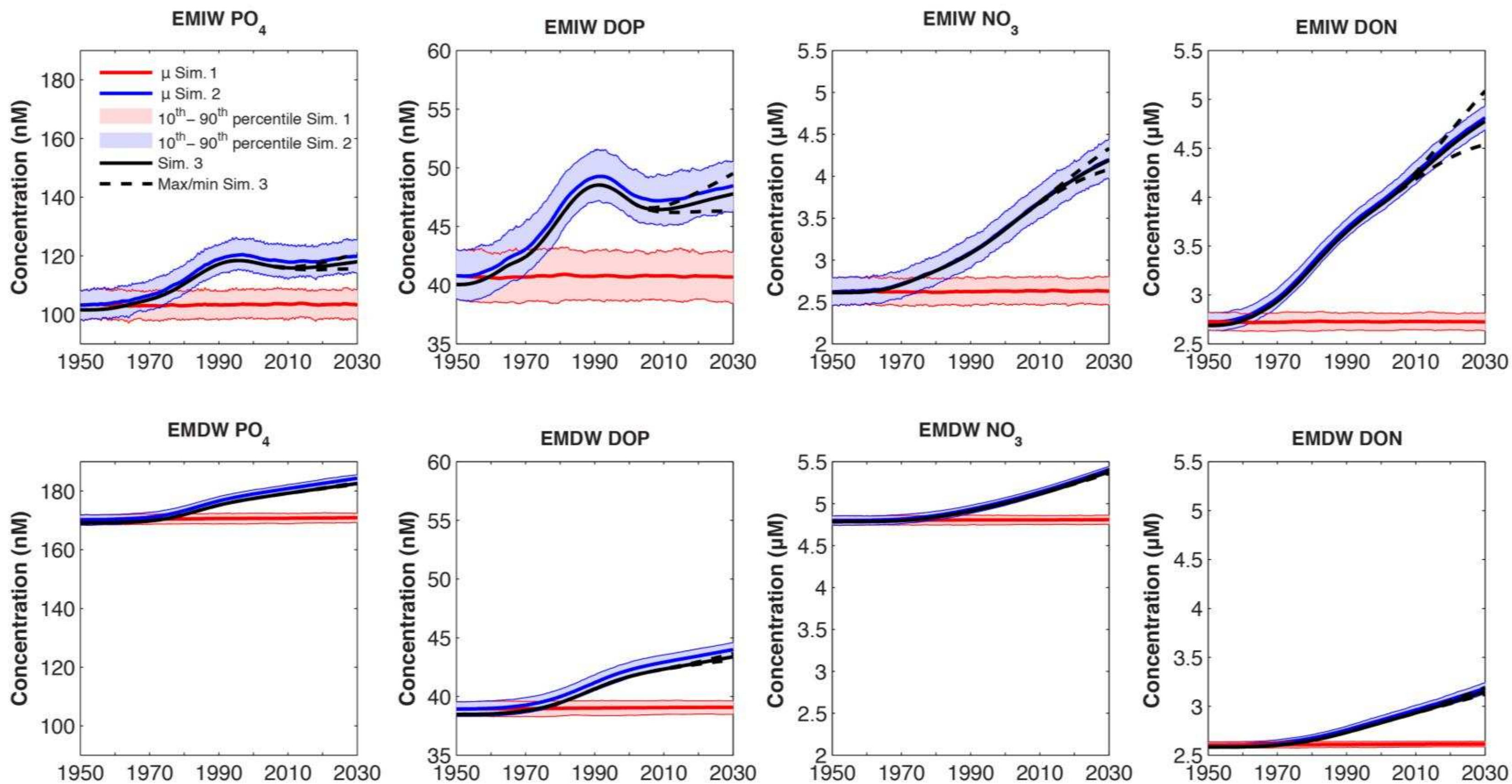

Figure 6: Trajectories of intermediate water (IW) PO_4 and NO_3 concentrations in WMS and EMS based on reconstructed deep water (DW) formation rates between 1960 and 2000 with constant reactive P and reactive N inputs (Simulation 4); variable (1950-2000) reactive P and reactive N inputs (Simulation 5); and imposing 5-year running average DW formation rates with variable reactive P and reactive N inputs (Simulation 7). Also shown are the trajectories for variable (1950-2000) reactive P and N inputs with constant thermohaline circulation (Simulation 3; red line). See text and Figure S3 for details on the historical DW formation rate reconstructions.

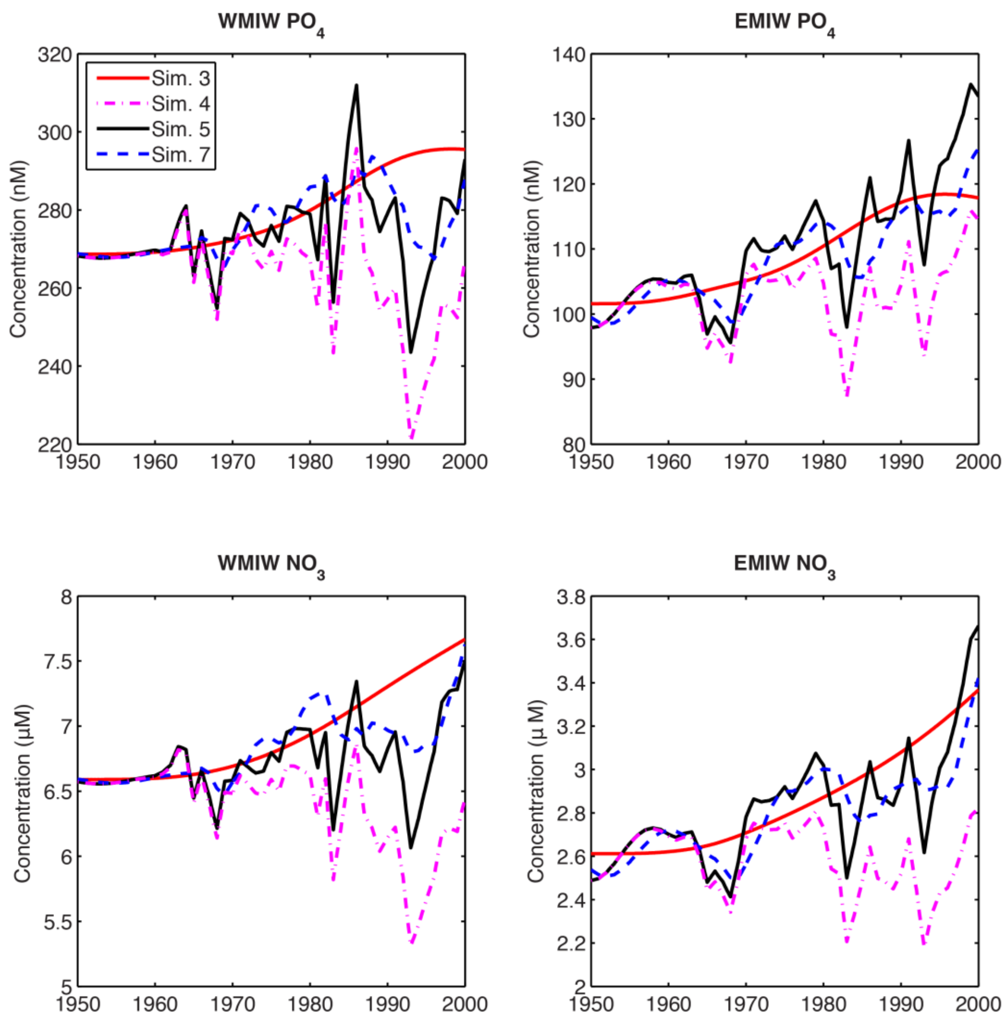

Figure 7: Same as Figure 4, but for the N:P ratios in the intermediate (IW) and deep water (DW) reservoirs of the WMS and EMS.

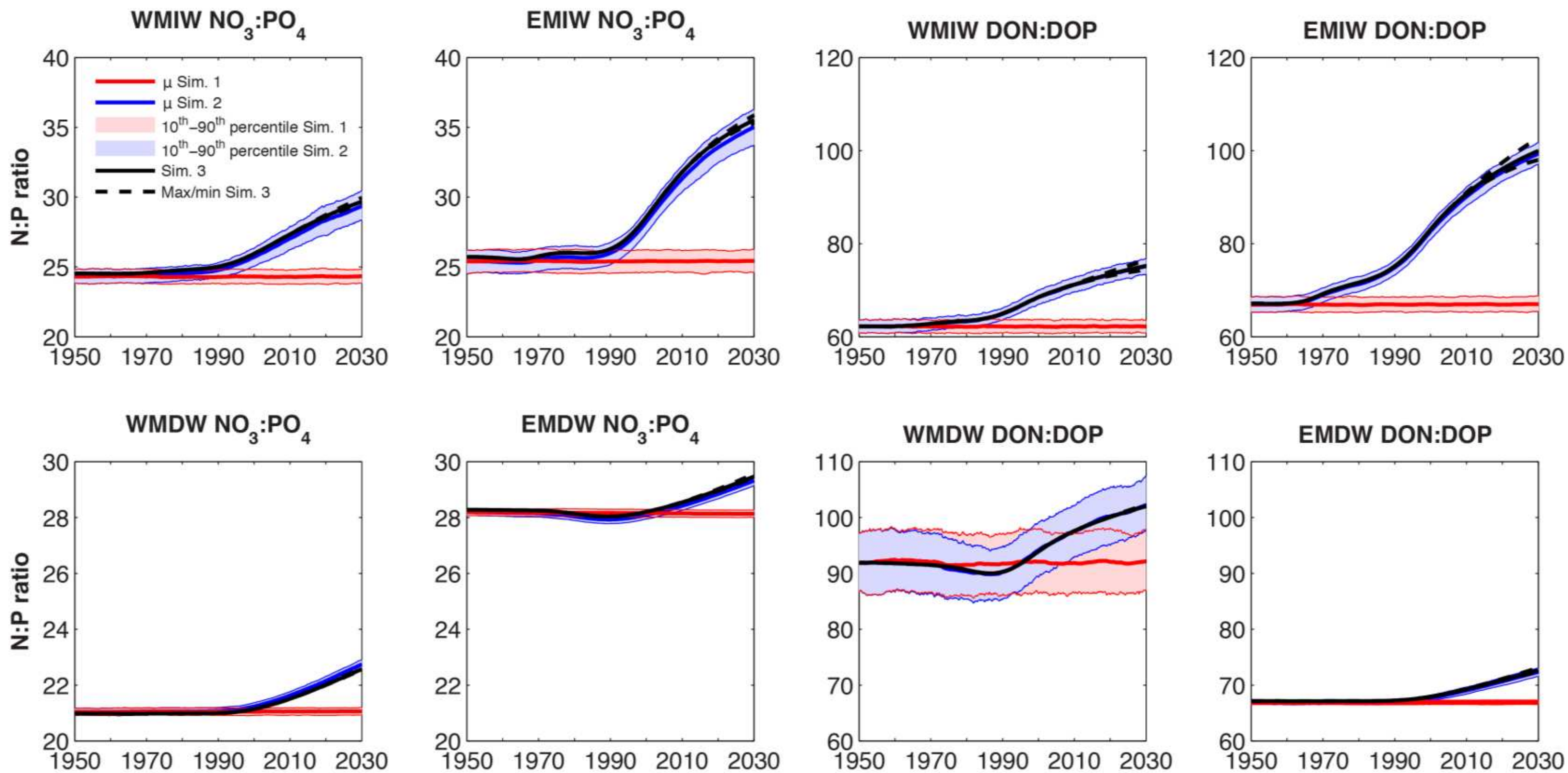

Figure 8: Same as Figure 4 except for annual primary productivity in WMS and EMS.

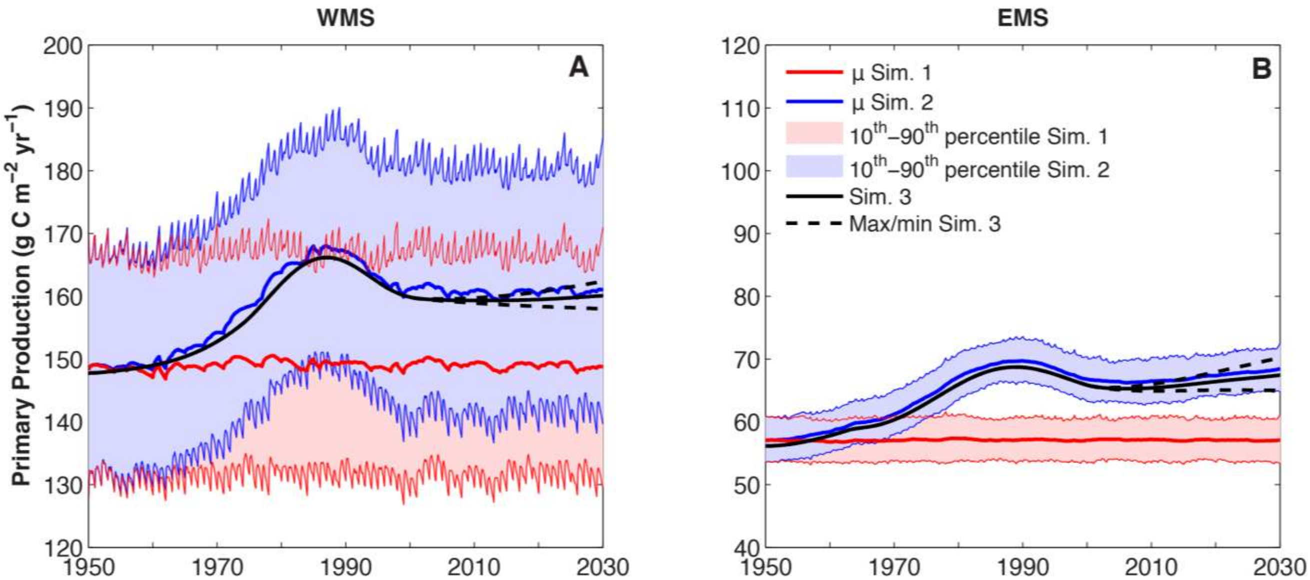

Figure 9: Fate of anthropogenic P and N supplied between 1950 and 2030 to the WMS (A and C) and EMS (B and D), expressed as percentages. Burial, denitrification (Denit) and outflow to Atlantic (Atl), EMS and WMS refer to the percentages of the total reactive P and N supplied, while accumulation in the water column reservoirs differentiates between the different chemical species of P and N

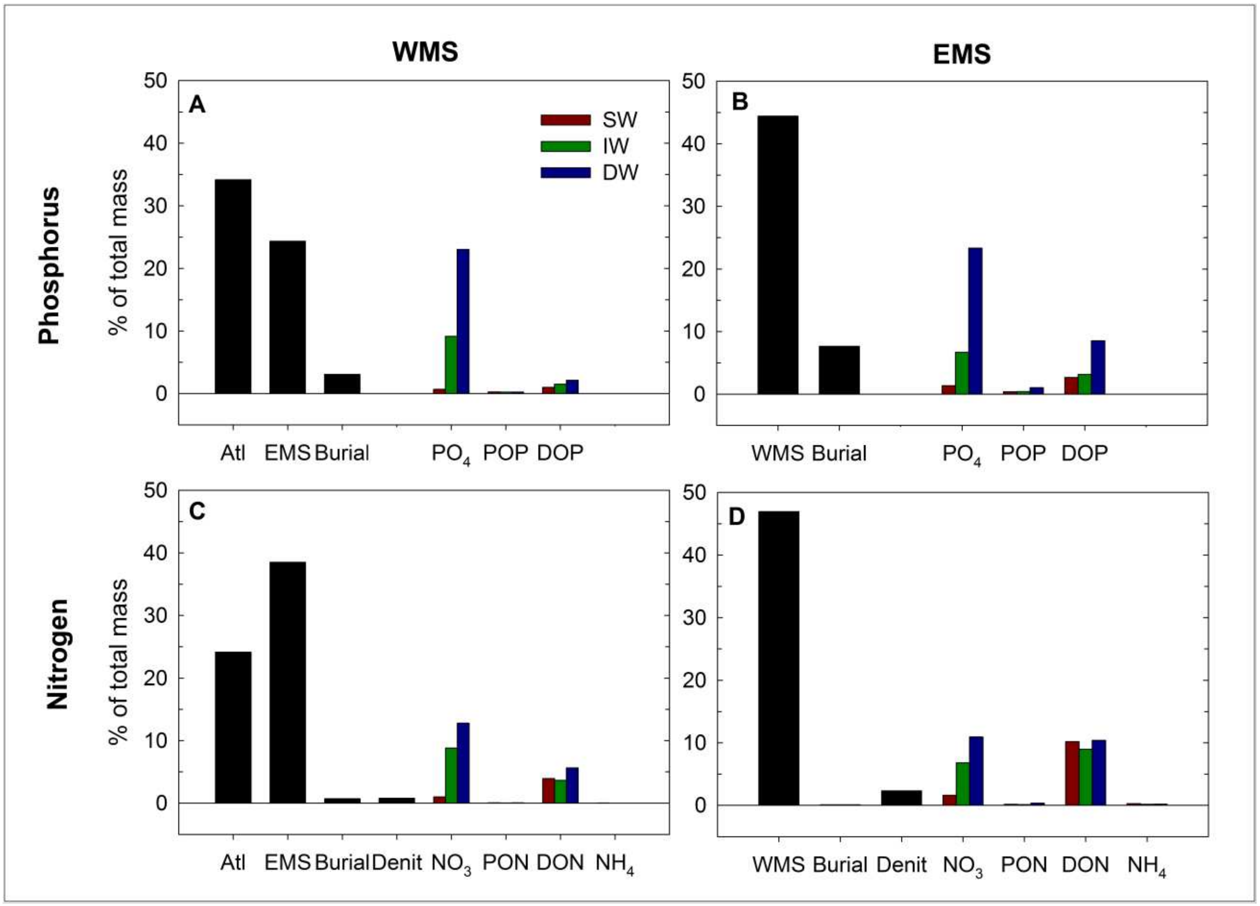

.

TABLE CAPTIONS:

Table 1: Summary of the methods used to calculate the 1950 to 2030 anthropogenic forcing functions applied in the mass balance model calculations.

Table 2: Model simulations combining the various circulation scenarios with constant or variable and reactive P and reactive N inputs.

Table 3: Parameters of deep and intermediate water formation used to initiate the random circulation scenarios. See text for details. [a]From Powley et al. (2016a)

TABLE 1:

Forcing function	Species	Method and data sources
Atmospheric deposition	PO_4	Deposition of leachable PO_4 in the WMS and EMS is assumed proportional to changes in acid availability in the atmosphere above the Mediterranean basin (Nenes et al., 2011), estimated through emissions of NO_x and SO_4 to the atmosphere in Europe, Africa and the Middle East. For 1950-2000 the forcing function is justified in Powley et al. (2014) and references therein. For 2000-2030 data are taken from Lamarque et al. (2013).
	DOP and DON	Deposition of organic matter in both WMS and EMS is assumed proportional to the relative change in 1) organic carbon emissions from biomass burning in the northern hemisphere over 1950 to 2000 (Powley et al., 2014 and references therein), and 2) anthropogenic global organic carbon emissions for 2000-2030 (IPCC, 2013).
	NO_3 and NH_4	Deposition estimates in both the WMS and EMS are calculated from the relative changes in 1) NO_x and NH_4 deposition rates in French alpine ice core records from 1950 to 2000 (Powley et al., 2014 and references therein) and 2) model predicted dry and wet deposition rates for NO_x and NH_4 from Africa, Europe, and former USSR and Middle East (2000-2030).
Rivers	P and N	Ludwig et al. (2009) report riverine inputs of P and N to the WMS and EMS for every 5 years between 1963 and 1998. We assume minimal changes in riverine P and N inputs from 1950 to 1963. The relative changes in riverine inputs from 2000 to 2030 are those of Ludwig et al. (2010) based on the Millennium Ecosystem Assessment Scenarios. The relative speciation of P and N are assumed to stay constant with time.
Direct wastewater discharges	N	Wastewater discharges are assumed proportional to the coastal population of each Mediterranean country (FAOSTAT, 2016), weighted towards each country's individual wastewater total N input into the MS (Powley et al., 2016b). A ±5% error is assigned to the 2030 population estimates to represent upper and lower limits.
	P	The N:P ratio of direct wastewater discharges is assumed to follow the same trajectory as the N:P ratio of riverine discharge.
SGD	NO_3 and NH_4	The change in inorganic N in SGD is assumed to follow that of inorganic N fertilizer inputs on land with a 30 year time lag (Powley et al., 2017). The forcing function is created using the relative change in total N fertilizer consumption rate in the EU for the WMS and in rest of the world for the EMS between 1920 to 1960 (Erisman et al., 2011), while nitrogenous fertilizer consumption rates per country (FAOSTAT, 2015a), weighted to regional GW discharges (Zekster et al., 2007), are used for the period 1960 to 2000.
	DON	The change in DON in SGD is assumed to follow the application of manure on land with a 30 year time lag (Powley et al., 2017). Manure application rates in the EU are used for the WMS, and in the rest of the world for the EMS, over the 1920 to 1960 period (Erisman et al., 2011) and for each individual country (FAOSTAT, 2015b) weighted to regional GW discharges (Zekster et al., 2007) for 1960 to 2000.
	P	Assumed constant with time as the 2000 P concentration in SGD is very small suggesting that P from fertilizer input is retained within the aquifers.
N_2 fixation	N	Assumed constant with time due to lack of correlation between nitrogen fixation and nutrient availability (Berman-Frank and Rahav, 2012; Sandroni et al., 2007).

TABLE 2:

Simulation	**1**	**2**	**3**	**4**	**5**	**6**	**7**
Randomized perturbations in circulation (constant mean): 1950-2030	✓	✓					
Constant circulation: 1950-2030			✓				
Reconstructed historical circulation (year by year): 1960-2000				✓	✓		
Reconstructed historical circulation (5-year moving average):1960-2000						✓	✓
Constant 1950 P and N inputs	✓			✓		✓	
Variable 1950-2030 P and N inputs		✓	✓		✓		✓

TABLE 3:

Area	Mean IW/DW rate of formation events (Sv)	Standard deviation (σ) of formation events (Sv)	Probability distribution function	Range (Sv)	% of years IW/DW formation occurs	Mean formation rate (Sv) (all years)[a]	Reference
	Years when IW/DW formation occurs				All years		
NWM	1.20	0.68	Lognormal	$0<x<3.3$	53	0.61	L'Hévéder et al. (2013)
Levantine	1.10	0.83	Normal	$x-\sigma< x<\sigma+x$	100	1.10	Vervatis et al. (2013)
Adriatic	0.455	0.25	Lognormal	$0<x<0.8$	80	0.32	Pinardi et al. (2015)
Aegean	0.069	0.08	Lognormal	$0<x<0.38$	62.5	0.04	Vervatis et al. (2013)